Chapter 3

Meristem Size and Phyllotaxis

3.1 Introduction

In the meristem of plants, leaves and flowers form around the periphery and are pushed radially outward as the cells of the meristem divide and expand. The angles between successive organs, called divergence angles, are fixed in place even as the shoot grows in length and circumference. In many plants, the relative positioning of organs around the shoot, called phyllotaxis, takes on a spiral pattern. This spiral is composed of divergence angles approximately equal to the golden angle of $\sim$137.5°, which has led many people to wonder about the mathematical nature of the pattern forming mechanism. Phyllotaxis has been studied and speculated about for centuries but with modern technology and methodology we can begin to unravel the complex phenomena underlying these beautiful patterns.

3.1.1 History of Phyllotaxis

Leonardo da Vinci was the first to suggest that the spirals found throughout the plant kingdom provide a fitness advantage. He suggested that the spirals maximize the number of leaves or flowers that can fit around the shoot to maximize the collection of sunlight and rainfall[1]. Johann Wolfgang von Goethe, the German poet and philosopher, wrote about the general pattern he observed where plants create a spiral pattern with their leaves[2]. Goethe had extensively written in "Versuch die Metamorphose der Pflanzen zu erklären" about the homologous nature of different organs through

the plant's development from the early cotyledons to the photosynthetic leaves to the petals and sepals of the flowers, deducing that they were all modifications of the same basic structure, specialized for different functions like reproduction. He speculated that the same phyllotaxis mechanism was used throughout the life of the plant.

More insight about the mechanism of spiral pattern generation came when Wilhelm Hofmeister proposed in 1868 that organ primordia form in areas of least crowding around the meristem. He suggested that the golden angle arose when successive primordia push on each other through physical forces, guaranteeing that the flowers would not form a straight radial line from the center of the meristem outward[3], similar to how spherical objects will pack with each layer being shifted horizontally from the last simply due to gravity and physical forces between the spheres.

Ten years later Simon Schwendener published the book "Mechanische Theorie der Blattstellungen"[4] in which he asserted that the different observed arrangement of leaves results from pressure exerted by each leaf on its neighbors, similar to Hofmeister's idea. He used a combination of diagrams and calculations along with a mechanical device which he constructed, essentially a specialized analog computer, to compute the forces experienced by leaves during development. While these devices were not built using knowledge of the biochemistry involved, they did provide a plausible mechanism for pattern formation.

Arthur Harry Church in 1904 furthered this mechanical line of thinking and proposed that the shoot apical meristem is the origin of the observed pattern, as opposed to the organs moving around the meristem after formation[5]. He introduced the concept of parastichies which were lines of force that traced the path of the organs down the stem and took on different wavelengths to produce the different observed phyllotaxis patterns. He named this "equipotential phyllotaxis" and created a very thorough theory of the parastichies, analogous to the theory of electromagnetism, with equations describing all the ways in which parastichy forces interact to produce phyllotaxis patterns. Additionally, he proposed many metaphysical theories about how life energy flowed through parastichy force lines. Ultimately he failed to realize that the observed phyllotaxis patterns could arise without the need for incredibly complex waves and force interactions around the shoot.

In the early 20th Century Robert and Mary Snow realized that all the proposed phyllotaxis models fell into one of two categories: either the position of the organ was predetermined by an unknown property in the stem or the positions of the organs were determined by physical contact with other existing organs. They suggested that if the latter model was correct then moving or removing older

organs should influence the positions of new organ primordia. This led to the first experiments on phyllotaxis. They surgically removed floral primordia in lupin plants and observed the formation of new primordia under a microscope[6]. In this experiment they determined that isolating a primodium caused the phyllotaxis spiral to reverse and form a new primordium across the meristem from where they would have expected it to form. As a result of this work the Snows developed the concept of "first available space", similar to what had been proposed by Hofmeister 60 years prior. In this theory new primordia form in the area with the widest gap[6, 7, 8].

Following up on the Snows' work, Claude Wilson Wardlaw performed microsurgery on the fern Dryopteris and arrived at a similar but not identical conclusion[9]. Wardlaw built on the "first available space" theory and proposed inhibitory fields emanating from each primordia. This proposal also built on the work of Johannes Schoute in 1913 who had also proposed that the patterning of organ placement involved chemical inhibitors[10]. Wardlaw suggested that the inhibitory field was not a "causal factor" but that new primordia tended to emerge at locations where the inhibitory field was weakest[9]. In this case, the most recently formed primordium was the source of the strongest inhibitory field so the next primordium formed across the meristem from the last. After Wardlaw's work, the idea of inhibitory fields stuck around and became an important factor in subsequent phyllotaxis models.

The British mathematician and WWII cryptanalyst Alan Turning picked up on Wardlaw's work and towards the end of his life developed his own mathematical models incorporating the idea of inhibitory fields. He published "The Chemical Basis for Morphogenesis" where he laid out differential equations describing reaction-diffusion systems that could explain the spiral partterns of phyllotaxis[11]. In this model, small random disturbances to the uniform initial state of the partial differential equations led to pattern formation. After initiation, the spiral pattern became steady.

The work of Hofmeister was later revisited by Stéphane Douady and Yves Couder. They built a system to test if the crowding theory could create the spiralling patterns seen in phyllotaxis. They added drops of ferrofluid (a liquid with microscopic magnetic solid particles in suspension) to a magnetized plate of silicone oil. The ferrofluid drops repelled each other and created spiralling Fibonacci patterns around the circular dish[12, 13, 14, 15]. Their observations showed that the ferrofluid phyllotaxis pattern was controlled by a single simple equation

$$G = \frac{V_0 T}{R_c} \tag{3.1}$$

where V_0 is the velocity, in this case determined by the magnetic field gradient, T is the frequency of the drips, and R_c is the radius from the center of the plate that the drop was placed. The resulting parameter G is the ratio of two length scales that affected the pattern of the ferrofluid drops: the radial displacement of the drops during one period (V_0T) and the size of the central region (R). Or put another way, G was related to the plastochrone ratio proposed by Francis Richards[16] which characterized phyllotaxis patterns with the equation:

$$a = \frac{r_{n-1}}{r_n} \tag{3.2}$$

or the ratio of radii of two successive organ primordia. G turned out to be related to Richard's equation by a simple natural logarithm:

$$G = \ln(a) \tag{3.3}$$

Douady and Couder concluded that all dynamic models where new primordia form in a position repelled by or inhibited by existing primordia will inherently give rise to phyllotaxis organization of Fibonacci order and spirals with angles that eventually converge on the golden angle — a phenomenon which minimizes the value of G[13].

Around the same time Paul Green was also working on the idea that phyllotaxis is controlled by geometric ratios but proposed that that chemical gradients or repulsive forces between primordia were not necessary. Green proposed a model where compression, tension, and shear in the outer layer of the meristem epidermis control the placement of new primordia[17, 18]. In this theory, stress and strain accumulated in the epidermis as a result of meristem cells dividing and expanding, pushing on all of the surrounding cells. The sites of buckling (out of plane deflection caused by in plane compression) are the sites where primordia form. Green concluded that this growth-dependent patterning was regulated at the level of the entire meristem rather than being a result of local forces. As the entire meristem grows approximately equal in all directions, wrinkles form similar to those observed in wet skin that expands when its keratin absorbs water. Luis Francisco Hernandez along with Green made computer models of these biophysical forces in the sunflower capitulum and were able to recreate observed phyllotaxis patterns[19].

Hernandez and Green explored this buckling model further *in vivo* by growing sunflowers in devices that constrained the growth of their meristems. These perturbations led to alterations of the phyllotaxis pattern that agreed with predictions made by their previous computer models[19].

They interpreted these results to mean that mechanical buckling was upstream of any biochemical process or tissue differentiation. Through an unknown mechanism, cells that are under increased buckling strain detect that strain and propagate a signal to alter the biochemical state of the cell and ultimately cause the transcriptional changes needed to create a flower or leaf.

The concept of strain and buckling in the meristem causing phyllotaxis patterns was further explored by Dumais and Steele around the year 2000. They experimented with making cuts in different parts of the sunflower capitulum and observing the reaction of the surrounding tissue[20]. When they made cuts at the apex of the meristem the wounds were pulled open, suggesting that the tissue was under tension. When they made cuts around the periphery of the meristem the wounds remained closed, suggesting that the tissue was under circumferential compression. The area of the meristem where primordia are formed was under compression which strongly bolstered Green's theory. Now that the buckling theory had experimental evidence supporting it, Patrick Shipman and Alan Newell expanded the concept with a thorough mathematical treatment and determined that the observed buckling patterns could be explained by the compression of a flat rigid sheet sitting on top of an elastic material[21, 22]. The overarching message from their work is that if the meristem is large enough such that the ratio of its circumference to the buckling wavelength is large then the deformations (sites of organ formation) arise as linear combinations of the cosine of the radial and circumferential coordinates multiplied by their respective wavenumbers.

Meanwhile, biochemical explanations for phyllotaxis also began to fall into favor. It had long been known that organ primordia fail to form in Arabidopsis plants with mutant auxin transporters[23]. But work in Cris Kuhlemeier's lab on both Arabidopsis and tomato showed that auxin is necessary and sufficient for the initiation of organ primordia[24, 25, 26, 27]. They demonstrated that by applying auxin in a waxy paste to the surface of the meristem in a location where a primordia was not expected to form led to the initiation of an organ in that location. Additionally they showed that blocking polar auxin transport by application of N-1-naphthylphthalamic acid blocks the formation of organs. Further, evidence produced by Marcus Heisler showed that auxin was being transported by the polar transporter PIN1 in such a way as to direct all the auxin in an area to a point where an organ primordium would eventually form, solidifying the concept of auxin accumulation being upstream of organ differentiation[28].

As you can see, two different paradigms for regulation of organ formation have emerged. One is mechanical and the other biochemical. Many questions remain to be answered. Is one right and one wrong? If one is wrong, is the supporting evidence just purely coincidental? If they are both

right, what is the nature of the connection between the mechanical and biochemical? Do biochemical signals lead to mechanical buckling or is it the other way around? Some progress has been made towards resolving this conflict. Marcus Heisler and Olivier Hamant showed that mechanical perturbation (laser ablation of cells in the meristem) led to the repositioning of auxin transporters in nearby cells[29]. Additionally, through a combination of experiments, image processing and mechanical computer modeling Richard Smith and colleagues were able to determine that mechanical forces can act as a feedback signal on meristem patterning affecting the biochemistry[30]. But while connections between the biochemical and mechanical have been made, critical pieces of the puzzle remain at large, particularly mechanisms for sensing strain and the pathway leading from auxin accumulation to strain.

In this work I seek to push our understanding of phyllotaxis patterning further by exploring the relationship of the meristem size to the divergence angles produced — a relationship suggested by the models in Chapter 2. This ties in closely with Douady and Couder's assertion that phyllotaxis patterns are a result of simple geometric ratios and more recently the work by Oliver Hamant and colleagues, who have also made careful measurements of meristem sizes[31]. By using advanced, modern measurement techniques I seek to quantify relevant geometric parameters in the meristem and compare those with the macroscopically observed phyllotaxis patterns.

3.1.2 Measurement of Phyllotaxis

There are two general strategies when it comes to measuring phyllotaxis. One is to measure divergence angles and plastochrons (the spacing between successive organs) of the siliques of mature plants. The other is to measure the divergence angles of primordia by looking at the meristem. Both of these strategies theoretically result in the same output but the measurements may not always be exactly equal as there is a lot of growth, potentially anisotropic, in between the time when primordia emerge and when the siliques have matured. In some cases, anisotropic growth in the stem can create a large disconnect between these two measurements as in the case of the bp-1 multant[32].

Much of the early work on phyllotaxis, such as that by Hofmeister, Schwendener, and Snow, was done by observing leaf primordia around the meristem using compound microscopes. Since cameras were not a staple in biology labs at that point in time, measurements were taken using eye-piece reticles and pictures of the meristems were sketched by hand. While this method did suffice, it left for a lot of guess work. The later additions of comparator reticles and photomicroscopy did help

but larger gains in accuracy were made with the development of the scanning electron microscope (SEM).

Beginning in the 1920's physicists experimenting with electron beams found they could steer the beams and detect the reflection, providing a method that, in theory, could create much higher resolution images than optical microscopy[33]. For many decades the technique was limited to specialized labs and was an experiment in itself. In 1965 the first commercial scanning electron microscope, the Cambridge Scientific Mark I Stereoscan, was produced and allowed non-physicists to make high magnification, high resolution, high contrast images of the surfaces of their samples[34]. One of the biggest innovations with this device was the development of long-life CRT phosphors that allowed images to be transferred from the CRT screen (which would typically only allow for temporary viewing of the sample) to photographic film. This meant images could be developed into photographs and features could be measured on paper with good accuracy and repeatability, since the magnification ratios of sample to CRT and CRT to film were known.

The first SEM images of plants, published in 1973, were taken by John Owens and Marje Molder who were looking at rates of mitosis in the meristems of conifers[35]. Shortly after, Paul Green also began using this technique to study the regeneration of stems from leaf tissue[36]. Other plant scientists picked up on this[37, 38, 39, 40] and by the mid 1908s SEM had become a routine procedure for making precise measurements of microscopic plant morphology, including divergence angles between successive primordia[41]. But while this tool provided very detailed images of meristem morphology it had its drawbacks — primarily that the samples have to be fixed under harsh conditions, dehydrated, and placed in a hard vacuum, which can distort some of the morphological features. Additionally, the specimen can only be viewed at one point in time since the process is destructive.

Another technique was developed in Paul Green's lab that preserved the plant tissue but also provided the high resolution of SEM[42]. In this technique a mold is made of the meristem using the same quick-setting polymers used in dental molds. From the negative mold a positive cast is made from a material that can be sputtered with gold and placed in the vacuum for SEM imaging. This technique preserves very fine details of the meristem, even small meristems like those of Arabidopsis, and is non-destructive to the plant. A series of dental molds can be made from the same specimen to track morphology over time. This method is still used today in situations where the non-destructive nature of the technique is critical and high resolution images of the tissue surface are needed[30].

Even with the benefits that SEM and dental molds have provided for measuring microscopic morphological features, there is still room for improvement. While SEM images appear to be three-dimensional since shadows are visible, the appearance of depth is an illusion. In machines with backscatter detectors, the electrons are returned to the detector after being reflected and the returning electrons are blocked in the same way that light would be, leading to shadows. But the images produced by the detector are still only two-dimensional. Measurements taken from these images can not take the z-axis into account.

Advances in light microscopy allow for high resolution fluorescent images of the meristem in three dimensions. In confocal microscopy, out of focus light (light not emitted from the focal plane) is blocked by a pin hole, allowing for samples to be optically sectioned by moving the sample through the focal plane and taking a two-dimensional image at each height. The only limit to resolution is the wavelength of the emitted light which, while not as great as SEM, is sufficiently good enough for measuring distances between organs in three dimensions in the meristem. It also provides a view inside the tissue rather than just the surface. Advances to the imaging techniques have actually allowed for resolutions below the diffraction limit[43, 44] but it has been the advances in 3D image processing that have made the largest impact on our ability to quantify the morphology of the shoot apical meristem[45].

In addition to measuring phyllotaxis at the microscopic level of the meristem, it can also be measured by observations of the whole plant. One technique that has been commonly used throughout the history of research on phyllotaxis is to take a picture from the top of the plant. Divergence angles can then either be measured on a printout (or developed photo) or on a computer using a digital image and basic microscopy software like Fiji[46]. This method provides the benefit of being quick and simple, although it is limited to the apical most leaves or flowers as they will obscure the view of those below. Another approach is to use a divergometer, essentially a protractor that can move up and down the vertical axis of the plant to measure the divergence angles visually. A third approach to this problem is to use tomographic techniques for constructing a 3D model of the entire plant. This would provide the benefit of producing divergence angles for the entire plant all at once instead of just a few as is the case with meristem microscopy and could potentially be faster than a divergometer.

3.1.3 Tomography

Tomography is an imaging technique where a three-dimensional image is created by taking multiple two dimensional image "slices". The medium can be radiation, sound or any other type of wave but in this work I will refer only to radiation. Typically, images are taken from multiple angles and a three-dimensional image is created through a process called tomographic reconstruction.

The first use of this technique was developed by an Italian radiologist who figured out that by moving the X-ray tube around a point of interest during the exposure, the point would become brighter while everything out of the focal plane would blur[47]. The use of a similar technique became regular practice in the 1950s where it was used on chest X-rays[48] of tuberculosis patients. Taking X-rays from multiple angles gave the doctors a precise location of lesions prior to surgery. For 20 years, X-ray tomography was limited to manually or semi-manually positioning the X-ray tube and film cassette around the patient to acquire the needed angles. Devices were constructed to aide in positioning the device at precise locations but the resulting images were inspected visually and a three dimensional image was not reconstructed except for in the practitioner's mind[49].

In order to make X-ray tomography the precise and ubiquitous procedure that it is today, new math and electronics were needed. Prior to the first use of X-ray tomography the mathematician Johann Radon proved that any function can be reconstituted using the infinite projections of that function[50]. Since starting with an infinite set is impossible, Stefan Kaczmarz developed techniques for numerically approximating the function using a finite set of projections. This method is called the Algebraic Reconstruction Technique and is represented by a single equation:

$$x^{k+1} = x^k + \lambda_k a_i \frac{b_i - (a_i, x^k)}{||a_i||^2} \tag{3.4}$$

Each pixel is represented by a vector x, the measured projections are b, and λ is a relaxation parameter to balance the accuracy and the number of iterations needed to achieve that accuracy. As more and more projections (images from a different angle) are added, the original function (the 3D object that is being reconstructed) is converged upon. This mathematical technique is the foundation of most tomographic reconstruction and not just limited to X-rays.

With the rise of digital computers and these mathematical methods, Godfrey Hounsfield was able to build the first computed tomography machine for which he was awarded a Nobel Prize. The innovations in this field also helped with progress with other types of 3D reconstruction. X-ray

crystallography which, although it measures scattering instead of absorbance, borrows some of the same math and positioning techniques and has made large advances in biology[51]. With advances in digital camera, optical tomography has also become a possibility.

Optical tomography is the technique where multiple images taken with a camera are combined to make a single 3D model of an object or scene. This can be done with multiple stacks of parallel slices as is the case with confocal microscopes or with images of the surface of opaque objects. In the case of confocal microscopy, Christophe Godin's lab developed a software package for reconstructing the cellular structure of meristems in 3D using confocal z-stacks taken from three different angles[52]. The process involves first identifying the locations of common landmarks in all the images by hand to create an initial approximate alignment. Then a rigid transformation (particularly a block matching algorithm[53]) followed by a pyridimal alignment algorithm[54] precisely aligns the images. The end result is that data from one image that was not captured in the another image (due to the angle and slice spacing) are all combined into a single image containing more structures than any of the individual images.

The same concept is used in optical tomography of opaque objects. An image taken from one side of the object will only capture information about the object that is visible on that side. Some features will be partially or completely obscured. By combining images from different angles a more complete model of the object can be built. In a rudimentary set-up the images would need to be aligned manually, which could be difficult considering the differences in working distances and background between images. To rectify this, modern optical tomography software makes use of reference targets that are printed with specific patterns to aid in determining the position of the camera in each image automatically, assuming the targets remain stationary. This technique is frequently used in forensics to create 3D models of a scene[55] or in surveys of archaeological sites[56].

In this work, optical tomography is used to capture and construct 3D models of whole plants with enough detail to extract the divergence angles between the successive siliques. With more advanced imaging techniques at both the microscopic and macroscopic levels and more advanced image processing techniques we should be able to make the most accurate measurements of plant morphology yet. This will aid in determining the relationship between meristem size and phyllotaxis pattern.

3.2 Methods

3.2.1 Plant Growth Conditions

Wild type and mutants lines as shown in table 3.2 were used. When plants were grown in soil, pots of soil were made using the following composition:

- 2 parts Sunshine Mix
- 2 parts SuperSoil Potting Soil
- 1 parts Vermiculite
- 1 parts Perlite
- 0.02 parts Marathon insecticide

Pots were arranged in flats of 12 pots and stored at 4°C for three days before transferring to a growth chamber with 24h illumination. Flats were given 1cm of water every 2 days.

Materials for Growing in Soil

- High wall petri dishes (Electron Microscopy Sciences, #64332)
- Sunshine Mix (McConkey Co, #SUNSM2)
- SuperSoil Potting Soil (SMG Growing Media)
- Vermiculite #2 Coarse (McConkey Co, #TRWVMIC26)
- Perlite (McConkey Co, #TRWPERL6)
- Marathon Insecticide 1% (OHP Inc, EPA #432-1329-59807)

3.2.2 Microscopy

Plants from one of the genetic backgrounds listed on table 3.2 were grown in soil as described in section 3.2.1. These plants were grown under continuous light until the shoots entered the reproductive phase and bolted. Flowers were removed with sharp forceps under a dissecting microscope. The meristem and approximately 5mm of stem were removed using forceps and placed in a glass slide. The slide was refrigerated for 15 minutes. This slows endocytosis, which would increase the background noise while imaging FM4-64.

High wall petri dishes were prepared with 1% phytoagar made with DI water. A 1mL solution of 5ug/mL FM4-64 in DI water was prepared from a 200ug/mL stock solution of FM4-64.

- 1% PhytoAgar
- 4.3g/L Murashige and Skoog Basal Salt Mixture
- 1mL 1000x concentrated Murashige and Skoog Vitamin Solution
- 30g/L sucrose
- 50ug/mL kanamycin monosulfate.
- 1L DI water

After the meristem tissue sat at 4°C for 15 minutes, 50uL of the FM4-64 solution was placed on each meristem using a 200uL pipette. The glass slide containing the meristems was placed back in the refrigerator at 4°C for another 15 minutes. Small holes were poked in the agar in the petri dishes. The meristems were removed from the slide and the drop of FM4-64 solution was removed with a Kimwipe. The Meristems were then stuck into the holes in the agar facing upward so the stems protruded into the holes, holding the meristems firmly in place. DI water was added to the petri dishes to a height 1cm above the top of the meristems.

Meristems in agar were imaged using a Zeiss LSM 510 laser scanning confocal microscope with a 63x 0.95NA Achroplan water dipping objective. The sample was excited using a single 488nm laser through a 488nm dichroic mirror which can excite both FM4-64 and GFP (only FM4-64 if not imaging KAN1). A 500-525nm bandpass filter was used to capture light from GFP and a 650nm longpass filter was used to capture light from FM4-64 simultaneously.

Images from this procedure were processed using the technique described below in section 3.2.3. Meshes generated in MorphoGraphX were analysed to find the locations of KAN1 cells so the boundary of the meristem could be determined.

3.2.3 Meristem Image Processing

The first step for importing the data into MorphoGraphX was to convert the z-stack into TIFF format. The easiest tool for this job is ImageJ or Fiji, which is a particular distribution of ImageJ with many useful plug-ins already installed. In this work Fiji was used in place of ImageJ but ImageJ can be used also. In that case a plug-in would need to be installed which allows ImageJ to read the

particular z-stack format, in this case an LSM file (LSMToolbox for Zeiss LSM files, Loci_tools for Leica LIF files, Bio-formats for Nikon ND2 or Zeiss CZI files).

In order for MorphoGraphX to interpret the image file correctly the first image in the series to be the top of the meristem. When the order was reversed the data was exported as a series of individual TIFF files rather than a multi-TIFF so the order of the images could be reversed.

Before beginning the image processing, some steps were taken to insure all the software was set up and our data was ready to be processed.

- ImageJ or Fiji was installed
- MorphoGraphX was installed. On Ubuntu this can be done through the built-in package manager.
- The x,y,z dimensions of the voxels from the image file metadata were retrieved.

3.2.3.1 Multiple TIFF Images

When exporting the image data from LSM files into a series of TIF images, the following procedure was used.

1. Open ImageJ or Fiji.
2. Click on *File*, then *Save As*, then *Image Sequence*.
3. Select the TIFF format and start the numbering at 0.
4. Click *OK*.
    - This will create multiple image files.
    - One file for each slice in the z-stack.

The following Bash script (OSX, Linux or Cygwin environments only) was used to reverse the numerical order of the TIF file names when needed. This assumes the files are named like "image3.tif". The second line of the script can be modified if the files are named differently. The script was copied into the same directory as the multiple TIFF files and run.

```
#!/bin/bash
image=( image*.tif )
MAX=${#image[*]}
```

```
for i in ${image[*]}
do
   num=${i:5:3} # grab the digits
   compliment=$(printf '%03d' $(echo $MAX-$num | bc))
   ln $i copy_of_image$compliment.tif
done
```

In order to import these TIF images into MorphoGraphX, the following procedure was used:

1. The MorphGraphX program was started.
2. In the top menu bar select *Stack* then *Stack1* then *Main* then *Image Sequence*.
3. Click *Add Files*.
4. Select all of the image files in the series.
5. Click *OK*.
6. Input the X, Y, and Z dimensions of the voxels in micrometers.
    - These data were available in the metadata associated with the original image file.
7. Click *Start* and the stack appears in the main window in a semi-transparent state as seen in Figure 2.2A.

3.2.3.2 Single TIFF Image

In order to export the data as a single multi-TIFF image, the following procedure was used.:

1. Click on *File*, then *Save As*, then *Tiff*.
2. Select the TIFF format and start the numbering at 0.
    - This created multiple image files, one for each slice in the z-stack.
    - This file was imported into MorphoGraphX.
3. Open the MorphoGraphX program.
4. Drag the TIFF file into the main window.
    - This opens a window where the X, Y, and Z dimensions of the voxels in micrometers are manually entered.

- These data were available in the metadata associated with the original image file.

5. Click *Start* and the stack appears in the main window in a semi-transparent state as seen in Figure 2.2A.

3.2.3.3 Building the Mesh

The same general procedure for building a mesh from a z-stack was used as described in Section 2.2.11.5.

3.2.3.4 Segmenting

When using the KAN1 reporter this method was used for detecting the meristem edge cells were segmented from the mesh

1. At the left side of the window, click the *Add New Seed* tool.
2. Hold hold *Ctrl* and *Alt* and use the mouse to click the interior of a cell.
3. Do this for each cell as seen in Figure 2.3A.
    - Each cell should turn a different color.
    - You can drag the mouse to color a larger portion of the cell interior.
    - This can help if the background noise is high.
    - Each time you click you are drawing with a new cell-seed.
    - If you have already picked the mouse up but want to keep drawing with the same seed, select the *Add Current Seed* tool and draw with that.
    - To revert back to making new seeds, select the *Add New Seed* tool again.
    - To erase a seed:
        (a) Click on the *Label Color* (the colored box at the top of the window). The color should disappear.
        (b) Choose the paint bucket tool.
        (c) Click on the seed that you want to erase.

- With a new seed, draw a circle around the area you want segmented as seen in Figure 2.3A.

4. In the *Process* tab, expand the *Segmentation* section.
5. Click on *Watershed Segmentation*.
6. Use the default parameters.
7. Click *Go*.
8. Wait for the segmentation to complete.
9. If you are satisfied with the segmentation, proceed to step 12.
10. If there are corners between the cells that are not assigned a color:
    10.1. In the *Process*, *Mesh*, *Cell Mesh* section select *Fix Corners*.
    10.2. Click *Go*.
    10.3. In the *Segmentation* section, choose *Watershed Segmentation*.
    10.4. Click *Go*.
    10.5. The corners should now be fixed.
11. If you are not satisfied with the smoothness of the boundaries:
    11.1. In the *Process*, *Mesh*, *Structure* section select Subdivide Adaptive Near Borders.
    11.2. Map the signal data onto the mesh again using the procedure described previously at step in the section "Building the Mesh".
    11.3. In the *Process*, *Segmentation* section select *Watershed Segmentation*.
    11.4. Use the default parameters.
    11.5. Click *Go*.
12. Expand the *Cell Mesh* section and select *Convert to Cells*.
13. Choose a value of 1μm for the *Minimum Distance* parameter.
    - This determines the smallest wall segment.
    - Smaller values increase the number of points in the final dataset.

- Larger values decrease the number of points but may miss small details in the cell boundaries.

14. Save the cell data.

    14.1. From the top menus, select the *Mesh* dropdown menu.

    14.2. Select *Mesh 1*, then *Export*.

    14.3. Choose *Cells* for the file type.

        - This creates a text file will coordinates of cell boundaries only.
        - The entire mesh data is not included.

    14.4. Click *OK*.

15. Save the mesh.

    15.1. From the top menus, select the *Mesh* dropdown menu.

    15.2. Select *Mesh 1*, then *Save*.

        - This creates a .mgxm file.
        - All of the mesh data is included.
        - This file can be used to re-load the mesh later.

    15.3. Click *OK*.

When errors are received while trying to create cells (step 12), there sometimes was a problem with the structure of the mesh. The following Python code was used to try to fix the problem. After running this code, the steps at 12 were used to build the cells again.

```
Mesh.Segment_Mesh(20000)
count = 0
while count < 2:
    try:
        Mesh.Make_Cells(1)
        break
    except:
        Mesh.Fix_Corners()
        Mesh.Smooth_Mesh(1)
```

```
        Mesh.Segment_Mesh(20000)
    count += 1
```

At this point the data is exported as a text file (as created in step 14). This file contains the coordinates of all the cell boundaries. This was used to locate the cells expressing KAN1 so that the edge of the meristem can be quantified.

3.2.3.5 Identifying the Saddle Point

In cases when the SAM boundary was determined via the saddle point method, the following protocol was used. The file as generated at the end of section was open in the following Python script that turns the mesh into a set of z-values representing the height of the meristem at each point.

```
fi = open("filename.mgxm","r")
lines = fi.readlines()
fi.close()

data = []
for line in lines:
    items = line.split("\t")
    zvalue = items[4]
    data.append(zvalue)

fi = open("output.txt","w")
for d in data:
    line.write("%s\n" % (d))
fi.close()
```

This file was then imported into Matlab. The following Matlab notebook was run to extract the locations of the saddle points.

```
clear all;

% Read the CSV file with z-values
filename = 'output.txt';
im = csvread(filename)
```

```
% Calculate gradients field
[nr,nc]=size(im);
[dx,dy] = gradient(double(im));
[x y] = meshgrid(1:nc,1:nr);
u = dx;
v = dy;
imshow(im);
hold on
quiver(x,y,u,v)

% Estimate critical points
Cx=diff(Image,4,4); Cx(end+2,:)=nan;
Cy=diff(Image,4,4); Cy(:,end+2)=nan;
[i,j]=find( Cx.*Cy<=0);
```

The point with the negative curvature was determined to be the apex of the SAM. The closest identified saddle point was determined to be the nearest primordia crease. The Euclidean distance through 3D space from the saddle point to the apex was used as the size of the SAM.

3.2.4 Divergometer

To measure divergence angles "manually," a divergometer was used. The divergometer used here is a device designed and built by Arun Sampathkumar. It is a device designed to measure divergence angles around the shoot of Arabidopsis plants. It uses moving parts and a protractor to measure the angle. See figure 3.1 for more details.

Mature but still green plants were cut just above the rosette leaves using scissors. The plant was mounted in the divergometer using the clips. The protractor was rotated to line up with the two siliques to be measured. The angles was read off and recorded in a notebook. The data were transcribed into Excel, where distributions were plotted.

Figure 3.1: Divergometer used for measuring divergence angles and plastochon distances. Left panel shows the entire device. Right panel shows a closeup of the rotating protractor.

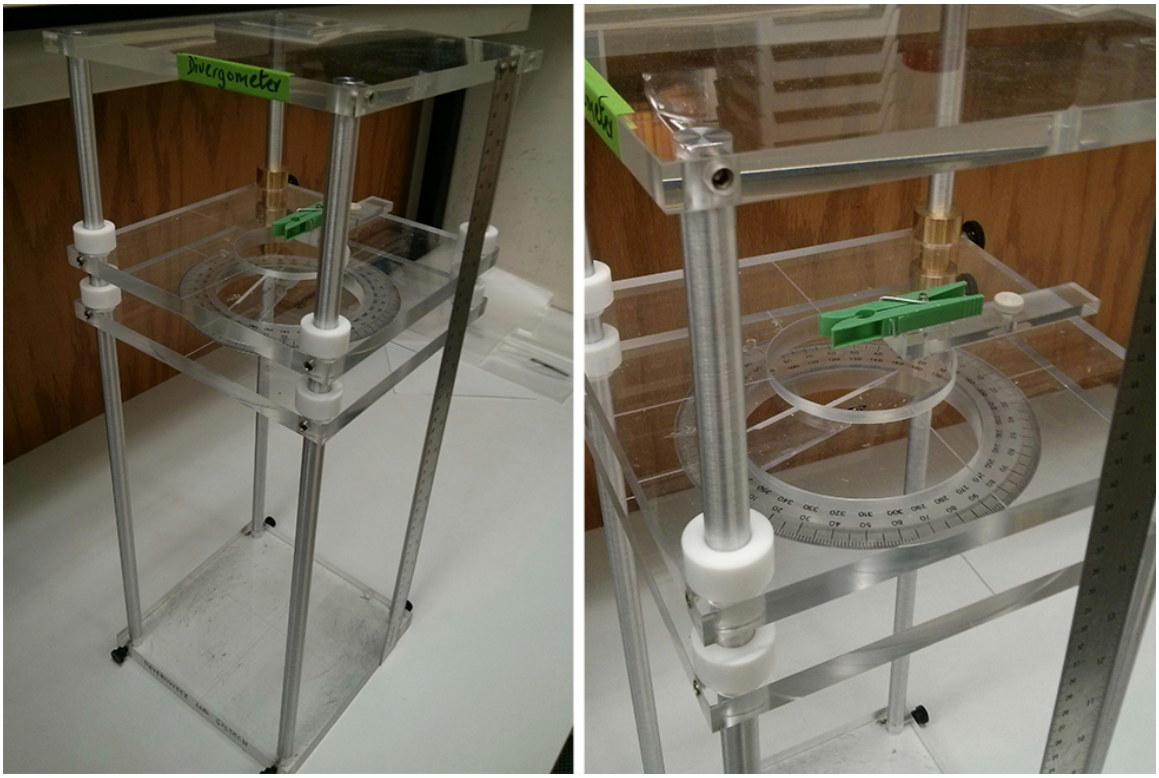

3.2.5 Tomography Photography

The shoots of plants grown in were cut off just above the rosette leaves with a pair of scissors. An orange bottle cap was turned upside down and filled with molten paraffin. Before the paraffin hardened the bottom of the shoot was submerged into the paraffin and held in place with a helping-hands device. After the paraffin hardened the cap with the plant was moved into a photography area.

The area had been set up with a black felt sheet to create a uniform background as seen in figure 3.10. Test patterns were printed out from PhotoModeler Scanner on an inkjet printer. The test petterns were cut out and taped to different locations on the black felt. A Nikon D80 camera with 35mm f/1.8 lens was mounted on a small tripod.

Six photographs were taken of each sample. The six photos were composed of three pairs of photos. Each pair was taken at the same angle but shifted horizontally by 10cm. One of the pairs was taken straight on and the other two pairs were taken at 45°to either side. The images were transfered to a computer via an SD card.

Figure 3.2: Photography strategy for tomographic 3D reconstruction. Six photographs are taken at three different angles. Each of the two photographs taken at the same angle are shifted 10cm perpendicular to the direction pointed by the camera.

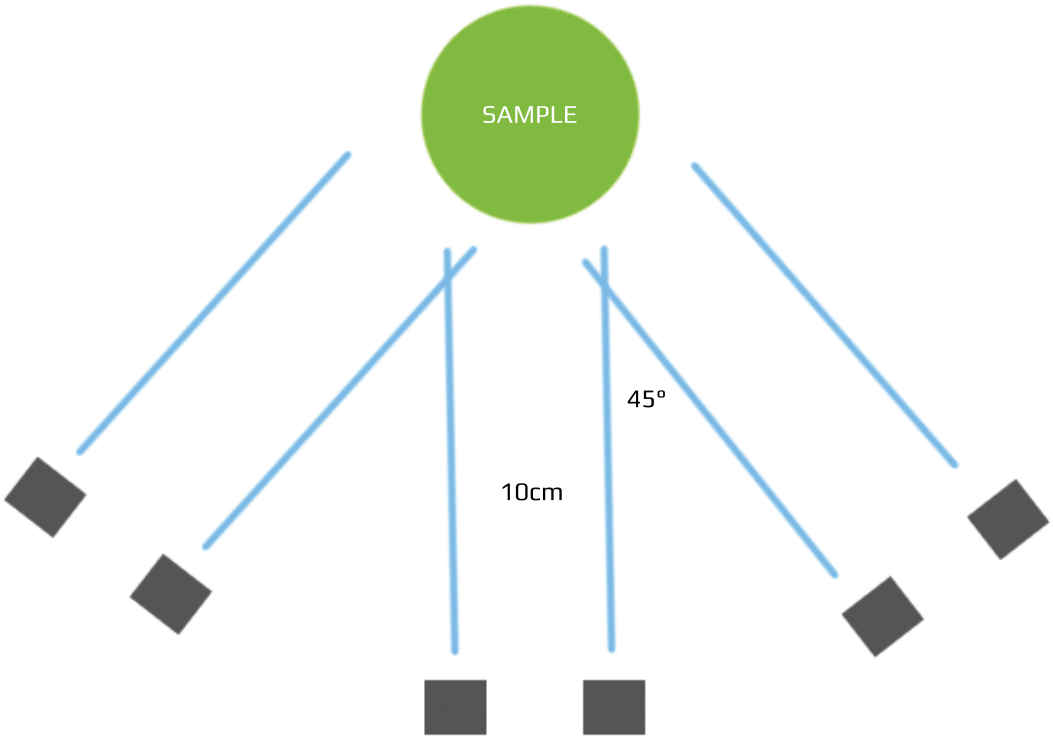

3.2.6 Tomography Software

Images collected as described in section were opened in the commercial software package called PhotoModeler Scanner v6.4. A calibration procedure was first run using six images of the test patters without any sample in the frame. This generated coordinates for the exact placement and orientation of each of the test patterns.

The six images of the sample were then loaded into PhotoModeler Scanner. Each image was processed to determine the location of the test patterns. Then a 3D model could be created. Once the model was finished being created, stray bits of mesh were removed manually using the touch-up tool. The 3D mesh was then exported for further processing in VTK format.

A custom software algorithm was developed to extract the divergence angles from the 3D model. This software was run on the VTK file and generated a series of divergence angles and platochrons in a text file. These numbers were then imported into Excel for further analysis.

3.3 Results

3.3.1 Meristem Size Via Fluorescent Markers

To measure the size of the shoot apical meristem, the edge of the meristem must first be defined as there is no clearly defined edge. One possibility is to use a fluorescent reporter driven by the promoter of a gene that is active around the region where we think the edge of the meristem might be. One candidate gene is KANADI1 (KAN1). KAN1 is thought to be expressed in a ring around the periphery of the SAM which would be useful.

A reporter was built (pKAN1::GFP-N7) by Marcus Heisler using the 5kb upstream promoter region of the KAN1 gene fused to a coding region for a nuclear localized GFP[57]. This construct was transformed into Arabidopsis thaliana ecotype Ler plants. The expression domain of this construct and the boundary of cells stained with FM4-64 were viewed using confocal microscopy. The images (Figure 3.3A) show a ring of expression around the periphery of the meristem in the first layer of cells in the epidermis and also one to two layers below that, depending on the exact location.

The region of KAN1 expressing cells is variable in that sometimes it flanks the primordia on the apical side, sometimes on the basal side, and sometimes on both. Initially, the locations of each nuclei were segmented using Fiji so exact measurements could be made in software. Depending

Figure 3.3: Segmenting KAN1 Expression. KAN1 expression forms a ring around the periphery of the meristem, primarily in the first epidermal layer but also in some deeper layers. In some parts of the SAM the KAN1 region is closer to the apex than other and the ring is broken in some regions. **A.** Maximum intensity projection of KAN1 expression in the shoot apical meristem. KAN1 labeled nuclei are shown in green. **B.** ImageJ segmentation of nuclei expressing KAN1 projected to a 2D plane.

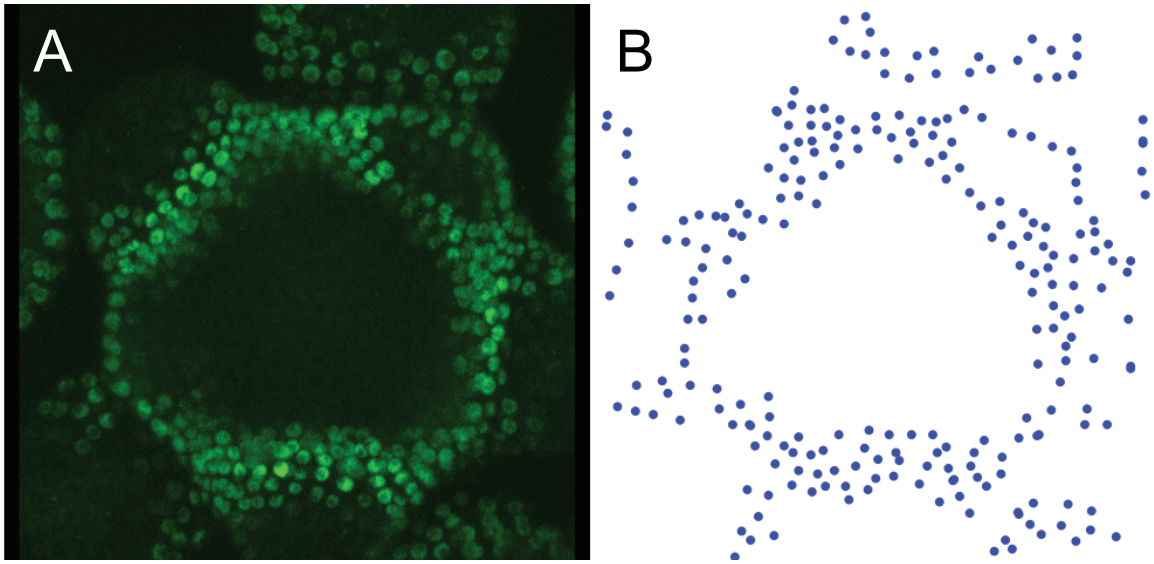

on the exact location in which we might measure from and the time the measurement is taken, the distance between the apex and that point can vary substantially(Figure 3.8), from 20μm up to 45μm or approximately the width if a flower primordium. This presents a problem for quantifying meristem sizes so a second approach was tested.

3.3.2 Meristem Size Via Topology

Using a geometric marker as landmark for measuring meristem size could excel over a fluorescent marker as the shape of the meristem is relatively stable whereas the KAN1 marker can be turned on and off in different regions through a dynamic process that is not understood. A new flower primordium is produced approximately every 12 hours so there will always be a crease in the meristem, a valley between the meristem and the nearest flower primordium, that is near the apex. In order to use this geometric feature as a landmark, I first need a computational method for mapping the topography of the meristem surface and extracting the 3D coordinates of the features of interest.

To generate a mesh representing the surface of the meristem, a confocal z-stack of the meristem stained with FM4-64 (lipophilic membrane marker) is taken. The z-stack is processed in the Mor-

Figure 3.4: The top layer of cells from a 3D confocal microsocopy z-stack mapped onto a surface generated from the cells in the image. Blue x's indicate maxima in the curvature and green o's indicate saddle points in the SAM topography. In order to determine the radius of the SAM, the distance between the maxima at the apex of the SAM and the nearest saddle point must be determined.

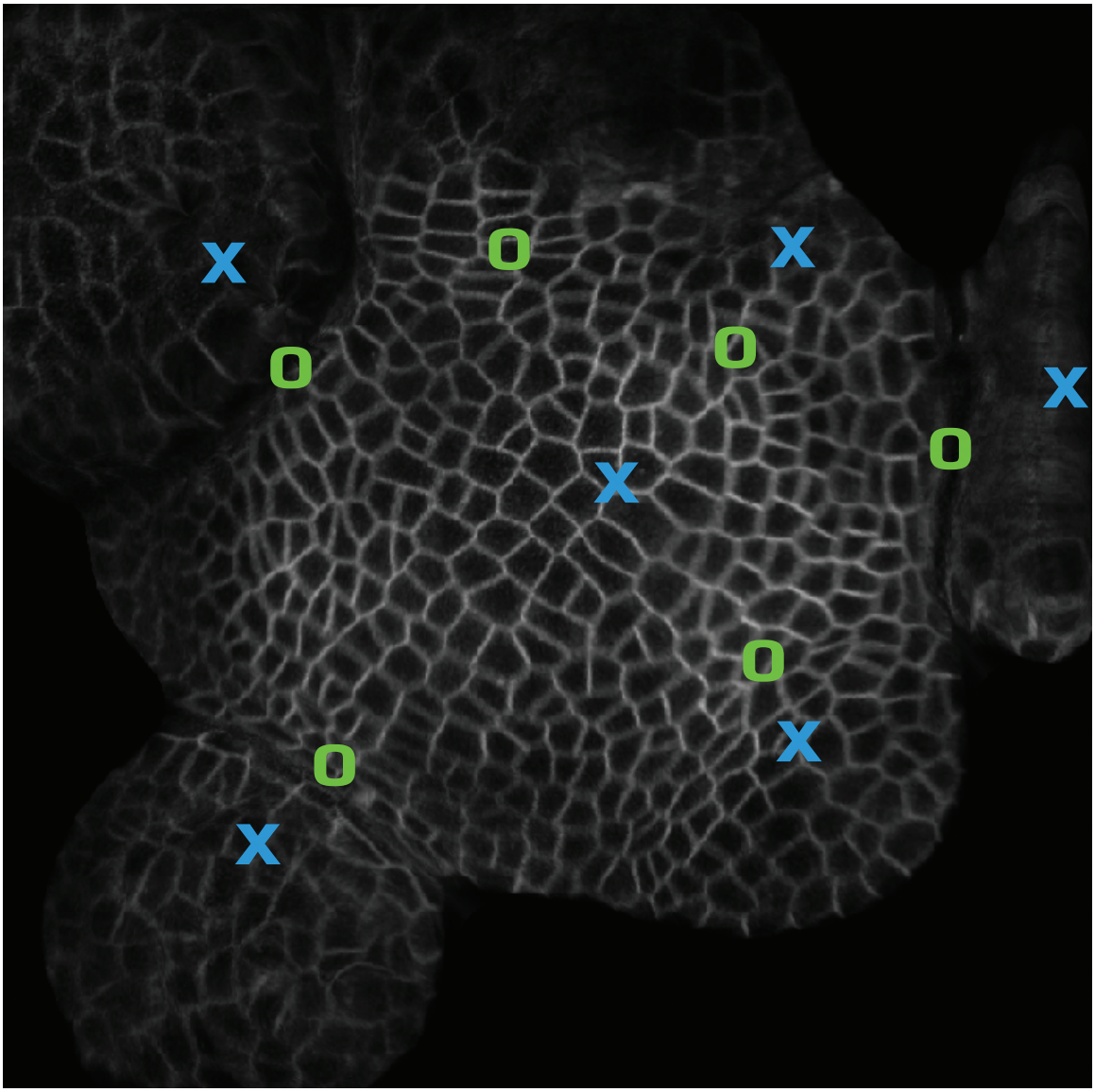

Figure 3.5: Starting with a z-stack of images from a confocal microscope, a heatmap of the height of the SAM is generated. **A.** 3D projection of the image data in MorphoGraphX. **B.** Mesh generated from the image data. **C.** High resolution heatmap generated from the mesh. 1 pixel for each pixel in the original image. The color is inverted so black areas represent higher z-values. **D.** Lower resolution heatmap generated using a reduction kernel.

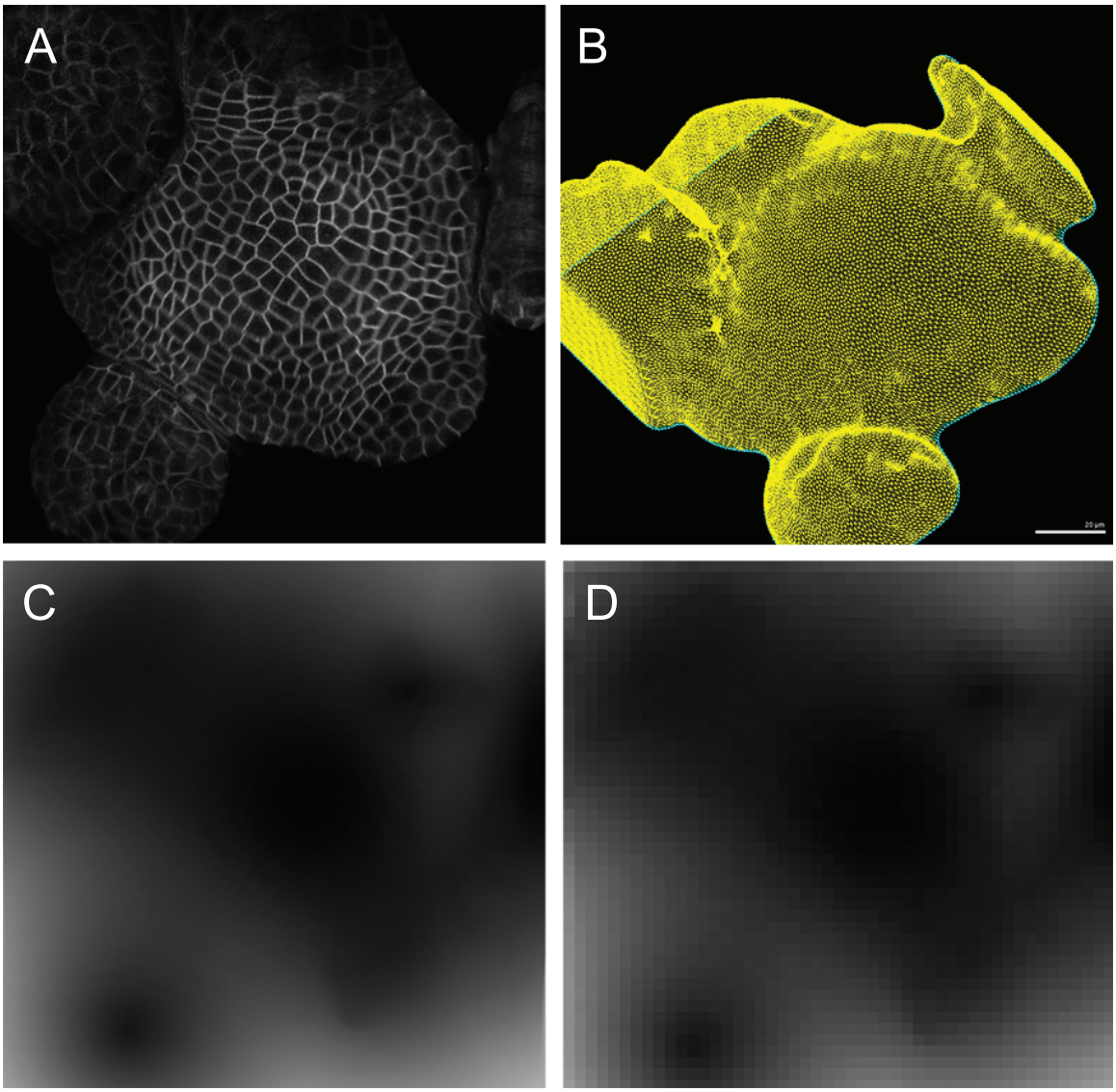

phoGraphX software pipeline to extract the meristem volume, positions of cells and finally a surface mesh as shown in Figure 3.5 panels A and B. The mesh is then smoothed to remove all small variations. The z-coordinates of each node in the mesh are isolated using a custom software algorithm, described in Section 3.2.3.5. The resulting scalar matrix represents the height at each point and can be visualized with a heapmap (Figure 3.5C). Since that resolution heatmap is not necessary for finding stationary points, the matrix is shrunk with a reduction kernel to a 50 by 50 matrix (Figure 3.5D). This matrix is then used for finding stationary points.

To find the stationary points a gradient field is first calculated (Figure). Since a true gradient can only be calculated on a continuous function, the field is numerically estimated with a short Matlab routine.

```
Cx=diff(Image,4,4); Cx(end+2,:)=nan;
Cy=diff(Image,4,4); Cy(:,end+2)=nan;
[i,j]=find( Cx.*Cy<=0);
```

This finds points where the slope crosses the zero line which is true for all stationary points, as in Figure 3.7. Each point is then classified as either being a maximum, minimum, or saddle point. The apex of the meristem is defined by the maxima nearest to the center of the image. This is dependent on the specimen being positioned in the focal plane properly during imaging so that the apex is actually the center most maximum. The saddle points represent the places where the primordia meet the meristem.

From here, the size of the meristem can be measured by looking at only the center most maximum and the nearest saddle point. These two stationary points are then mapped back to the original surface mesh in 3D. The distance between these two points on the mesh is then calculated using Dijkstra's algorithm[58]. This algorithm finds the shortest path between two nodes in a graph by making a tree of the connectivity of the nodes starting from one node and throwing out longer paths to any node as it proceeds. The distance between the two points in 3D along the surface of the meristem is calculated by adding up the length of each edge in the shortest path. This method provides a way to measure meristem size in a repeatable, although time consuming, way.

3.3.3 Comparison of Meristem Measurement Methods

To compare the merits of both methods, 20 plants of Ler ecotype containing the pKAN1::GFP-N7 construct were grown. The meristems were dissected and stained with FM4-64 and confocal z-stacks

Figure 3.6: Gradient map calculated from the heatmap in figure 3.5D. Gradient is calculated from the scalar field using a local approximation method in Matlab. A topological map, also generated from the same heatmap, is overlaid on top of the gradient vector field.

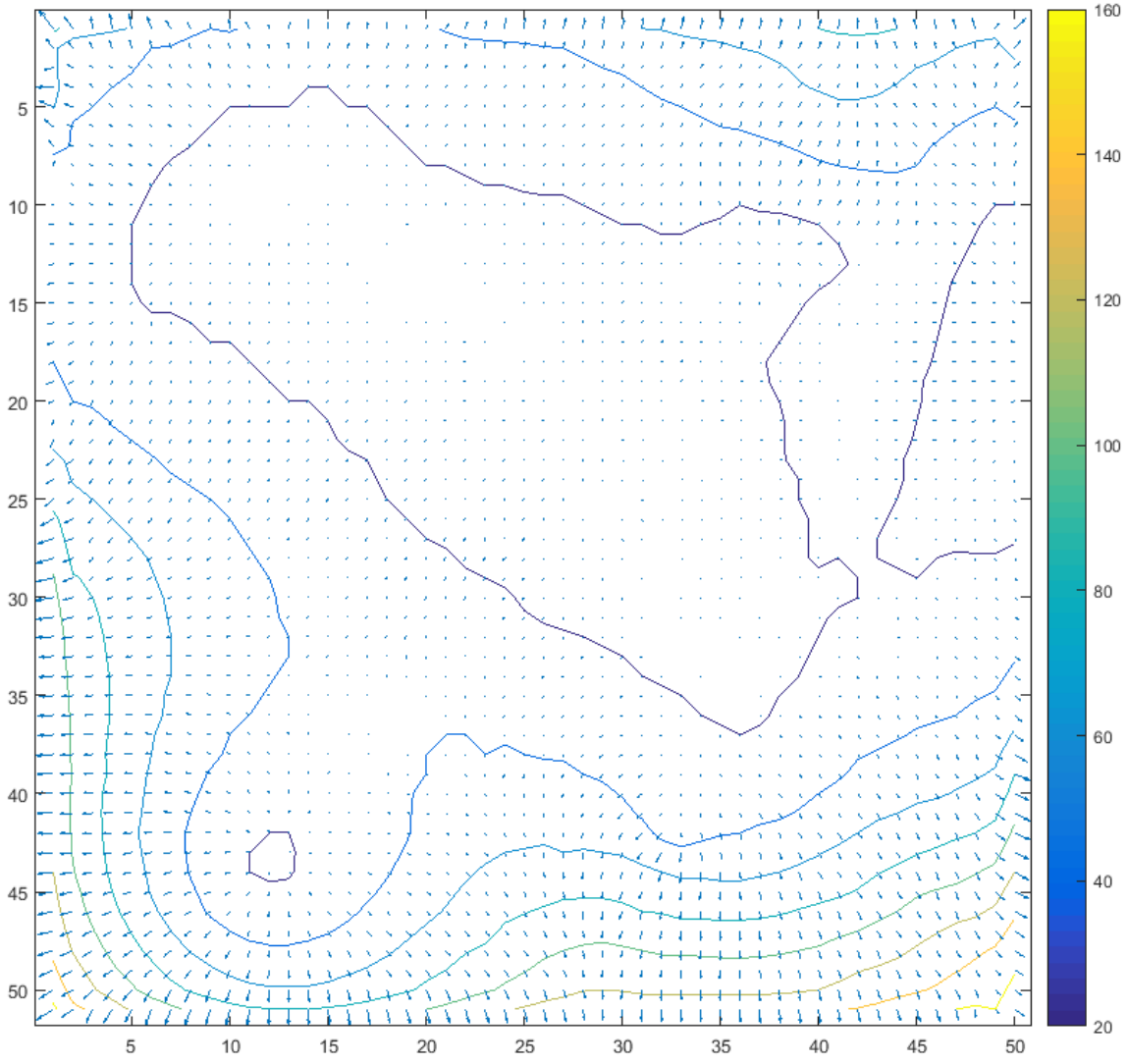

Figure 3.7: Critical Point Map. **A.** All critical points plotted on the topological map, including both maxima and saddle points. Lines represent the height of the tissue. **B.** Two critical points of interest of interest overlaid on meristem projection. Lowest point is the maximum at the apex of the SAM. Highest point is the saddle point nearest the apex (the lower point).

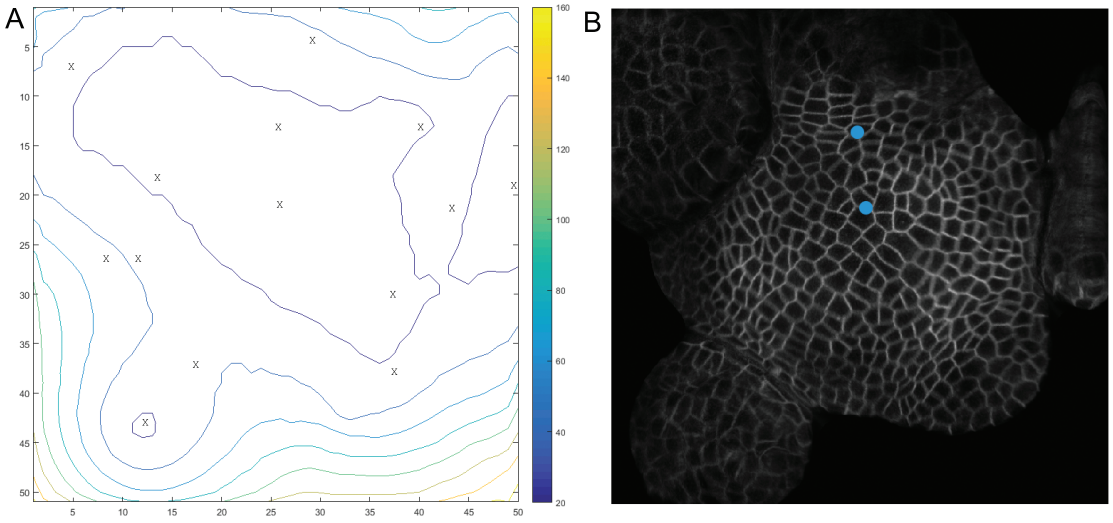

were taken of each meristem. Each image was processed with both methods. The resulting data in Figure 3.8 shows that both methods produce almost the same mean radius (32.5μm and 34.1μm), although this could be coincidental. But the variability using the fluorescent method is much higher, 6.8μm vs 2.2μm standard deviation.

There is a possibility that given a sufficiently large sample size the means of both methods will still remain nearly the same. In that case either method could be used if the mean value is all that matters. But the closeness of the means could be a coincidence. Given that the geometric method produces a much lower variability I am inclined to trust this method to produce results that represent reality more accurately and precisely. The geometric method takes significantly more time to complete each sample at approximately 5 hours compared to approximately one hour with the fluorescent marker method. But given the increase in apparent accuracy it is a worth-wile trade off. The rest of the measurements of meristem size in this study were done with the geometric method.

3.3.4 Measuring Phyllotaxis with 3D Tomography

Before starting this study my standard method for measuring phyllotaxis divergence angles was with a divergometer (see Figure 3.1). The accuracy of this method is dependent on the best judgement of

Figure 3.8: Comparison of SAM sizes of wild type plants using the fluorescent marker (KAN1) method and the saddle point method. 20 plants in the sample. Both methods produce very similar mean values. The fluorescent reporter method produces a much higher variability than the saddle point method so it was not used in the rest of this study. Error bars represent one standard deviation.

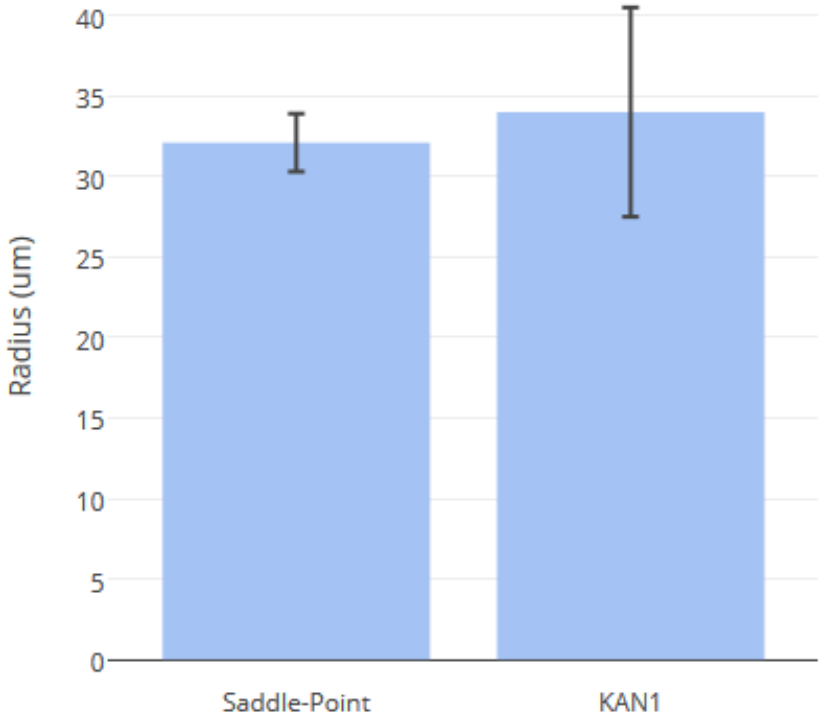

Figure 3.9: Comparison of the radii of SAMs within wild type and various mutant lines. The saddle point method was used rather than the fluorescent marker method. Many of these mutants show a deviation from the wild type radius. Some mutants have a wider variation, *wig-2* in particular, not due to measuring methodology but due to actual differences between individual specimens.

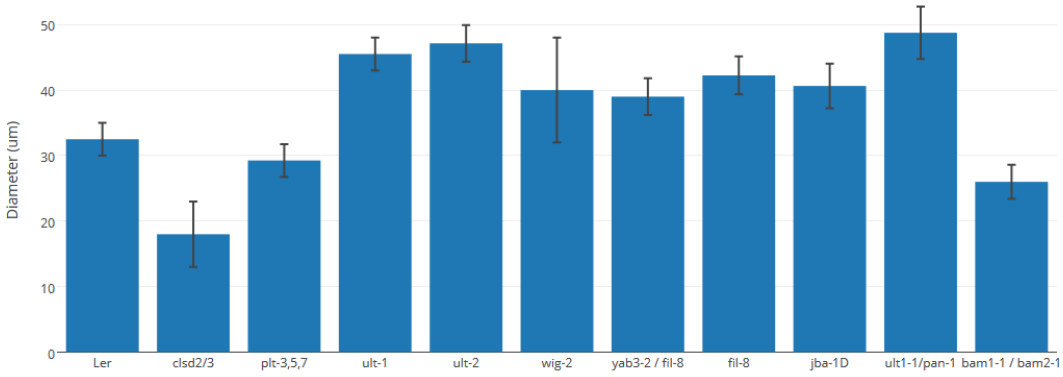

Figure 3.10: A plant mounted in a paraffin base and displayed in front of black felt for photography. The strips of paper next to the specimen are reference targets used by the tomography software to determine the orientation of the camera and the specimen. The area outside of the reference targets is ignored.

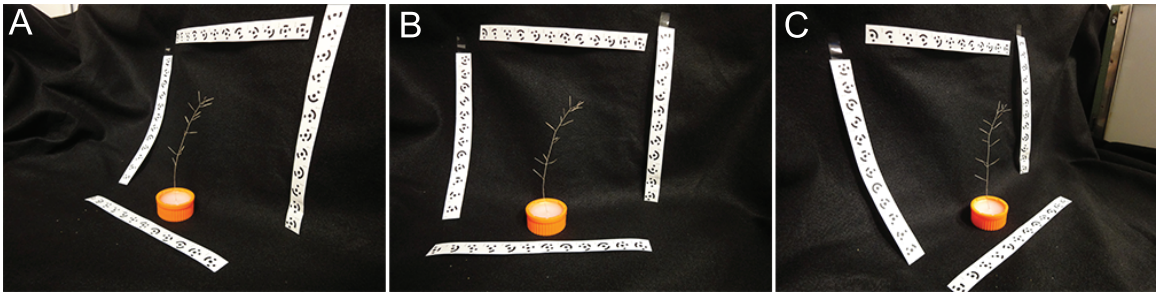

the operator when measuring the divergence angles on the protractor. Additionally, it requires a lot of tedious work and about 45 minutes per plant. To make this process more repeatable and accurate I explored using 3D optical tomography as an alternative method to the divergometer.

The tomography software Photomodeler Scanner was the primary software used. I generated optical reference targets which are unique circular patterns that can be recognized by the software to determine the location of the camera between each photograph. Each plant was photographed six times from three different angles (Figure 3.2). The images were loaded into Photomodeler Scanner and a 3D triangular mesh model was generated. These meshes were edited in MeshLab to remove any extraneous object such as the base used to hold the plant in place and any background objects that were picked up by the software. Once the mesh was devoid of any objects besides the plant, the new mesh was exported. The clean mesh was then processed with a custom algorithm which identified the shoot vs siliques and measured divergence angles between siliques.

This method produces results very similar to those of the divergometer. Figure 3.12 shows the phyllotaxis sequence for a single plant processed measured by both the divergometer and optical tomography. The divergence angles are often with 5°. Consequently I am confident in the accuracy of the optical tomography method but it has drawbacks. While taking the pictures of a single plant take about two minutes, the processing can take hours per plant. This is dependent on how much editing the mesh needs and how easily the custom software can identify the siliques. In situations where a silique sticks above the top of the shoot, the software will identify the silique as the shoot and the shoot as a silique which means the software must be manually forced to change its identifications. This is time consuming to the point where the divergometer measurements are quicker. Since both methods produce comparable numbers and the divergometer takes less time, the divergometer is the preferred measurement method.

Figure 3.11: An example of the software used to tomographically construct a 3D model of a plant, PhotoModeler Sanner v6.4. Raw photographs are loaded into the software. The software used the reference targets to align the images and generate a 3D model, shown in the top right panel. The color data can be mapped back to the surface of the model. In this case, the model was exported as a VTK mesh for further analysis.

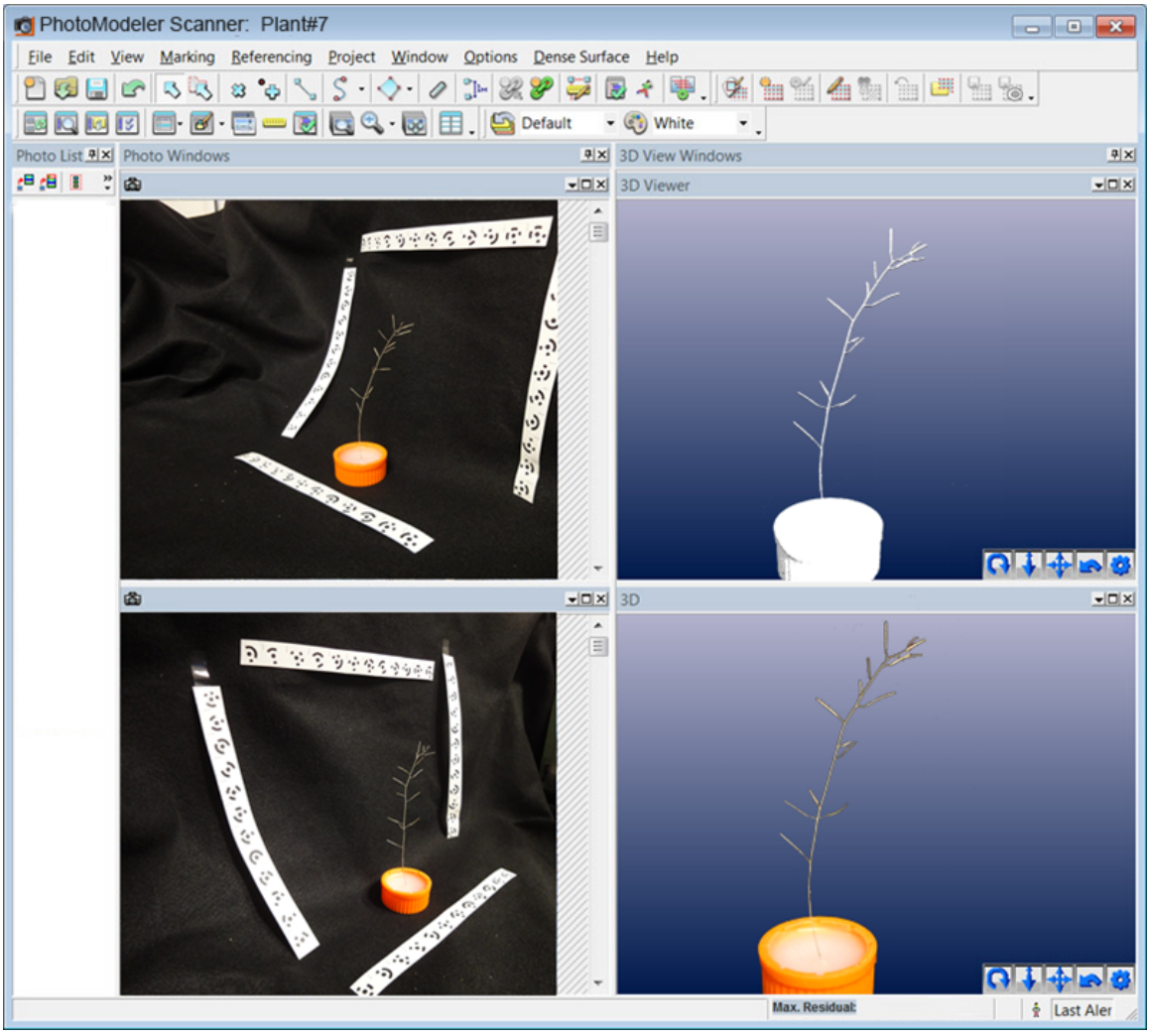

Figure 3.12: Comparison of data produced using two methods on the same sample. Orange shows the sequence of divergence angles produced using photographic tomography. Blue represents the same sequence as measured with a divergometer. Both methods produce very similar numbers, often within 5°.

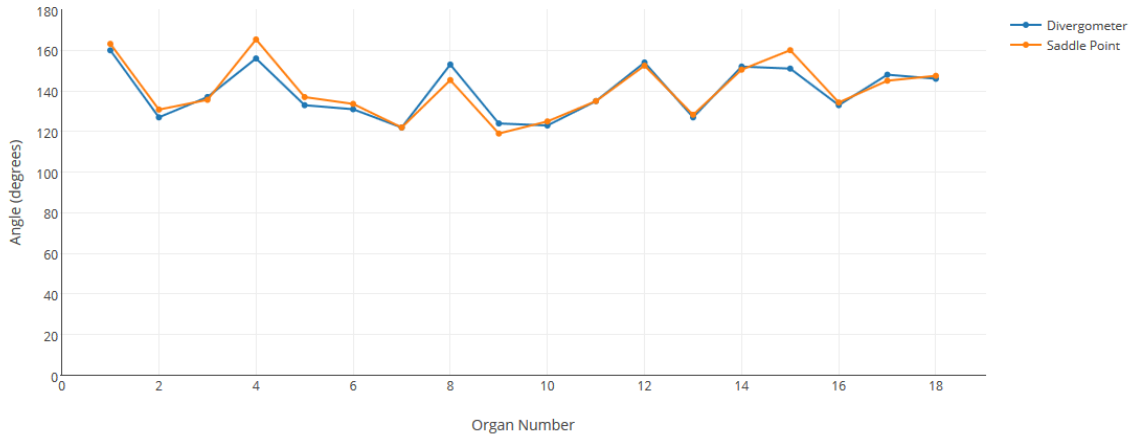

3.3.5 Mutant Phyllotaxis Comparison

As previous work has suggested, the size of the meristem plays a part in determining the observed divergence angles, at least in purely physical models[12, 13, 14, 15]. If this is true then altering the size of the meristem should result in altered divergence angles. To determine if there is a correlation between meristem size and phyllotaxis divergence angles I measured these two traits in 11 different genetic lines, which are listed in table 3.1. For measuring the meristem size I used the geometric method and for measuring phyllotaxis I used the divergometer.

The mean meristem radius of the various mutants is highly variable between the selected lines (Figure 3.2). This is not surprising as they were selected because the literature on these lines suggested they had meristem sizes different than wild type. The mean divergence angles on the other hand did not change much. For example, the bam1-1 / bam2-1 double mutant had a mean meristem radius of 26μm but the mean divergence angle is 134°, which is only a few degrees away from the "golden angle" of 137.5° and only 1° away from what wild type was measured to be in this study. The same goes for lines with larger meristems and those with smaller meristems.

The only obvious exception to this is the clsd2/3 line which had a mean divergence angle of 188°. The meristem of this line is very small, produces fewer flowers than most others, and emerges in a highly irregular pattern. In wild type plants, once the phyllotaxis spiral is initiated going either clockwise or counter clockwise and each successive flower follows the same handedness. Sometimes

Table 3.1: Genetic lines used in this study.

Mutant	**Note**
Ler	Wild type
csld2/3	Cell wall biosynthesis
plt-3,5,7	Transcription factor
ult-1	Transcription factor
ult-2	Transcription factor
wig-2	Farnesyl-transferase
yab3-2 / fil-8	Transcription factors
fil-8	Transcription factor
jab-1D	Transcription factor
ult-1 / pan-1	Transcription factors
bam1-1 / bam2-1	Receptor kinases

the handedness switches in the middle of growth but the switch is clear because all the flowers after the switch have divergence angles close to 137° measuring the other direction. In csld2/3 mutants the handedness switches periodically and it is not easy to determine if there has been a switch because the pattern is so erratic to begin with. Many flowers emerge with a 180° divergence angle, which also makes determining the handedness of the phyllotaxis pattern difficult. There is certainly an element of subjectiveness when it comes to determining which direction to measure the angles in this line. The scatter plot in Figure 3.15 shows there is not much correlation between mean meristem radius and mean divergence angle.

Looking at the distributions of the divergence angles in each line tells a different story. While many of these lines have a very similar mean divergence angle, the distribution varies much more (Figures 3.13, 3.14 and 3.15). In wild type there is a narrow distribution around the mean with a few points up in the higher values. In csld2/3 there is actually two peaks; one around 200° and another around 130°. The lines with larger meristems tend to have a wider distribution around the mean with more outliers in the higher value range compared to wild type.

3.4 Discussion

The plyllotaxis pattern of plants has been admired and studied for centuries. Early studies were teleological or descriptive in nature and any speculations about the underlying mechanism were arrived at from a top-down approach. It has not been until recently that we gained enough understanding of the molecular mechanisms to make sense of these patterns from first principles. It has been advances in our understanding of polar auxin transport that have lead the way towards understanding this

Figure 3.13: Left column: Distributions of divergence angles for each genetic line, binned in groups of 10°. Right column: A single example of the sequence of divergence angles for a single plant in each line. Plots show only the first 16 siliques to keep the axes equal.

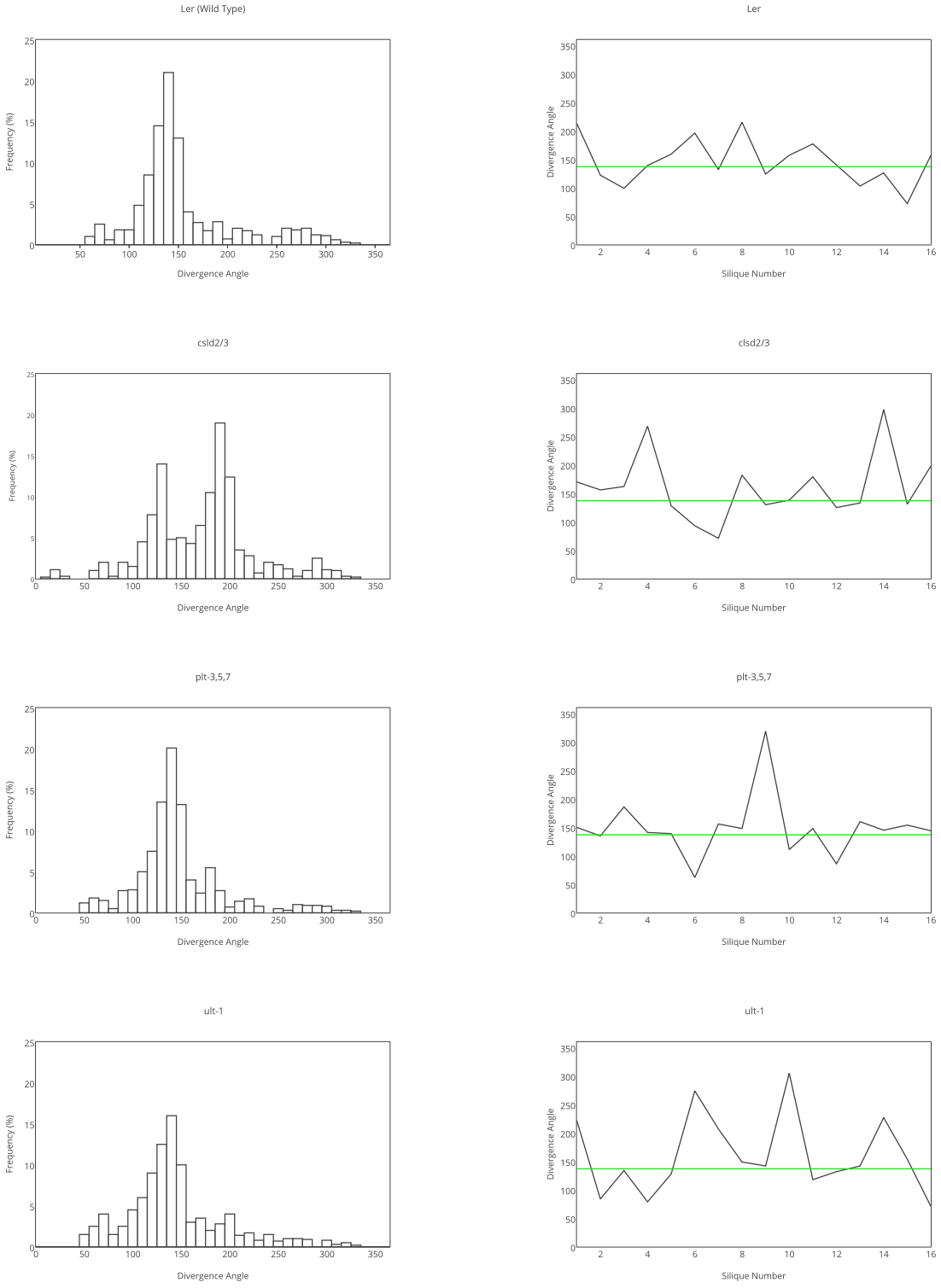

Figure 3.14: Left column: Distributions of divergence angles for each genetic line, binned in groups of 10°. Right column: A single example of the sequence of divergence angles for a single plant in each line. Plots show only the first 16 siliques to keep the axes equal.

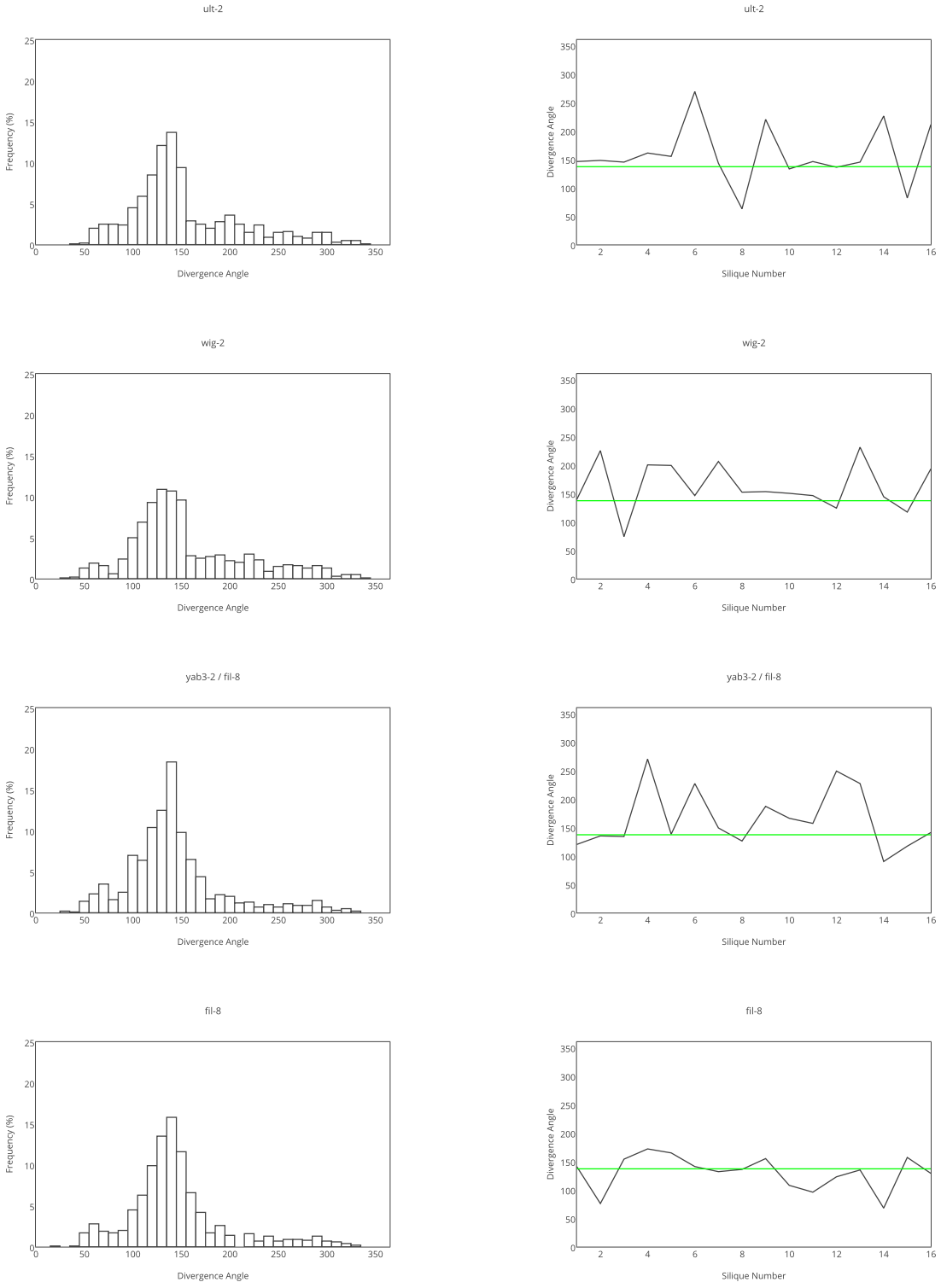

Figure 3.15: Left column: Distributions of divergence angles for each genetic line, binned in groups of 10°. Right column: A single example of the sequence of divergence angles for a single plant in each line. Plots show only the first 16 siliques to keep the axes equal. Bottom: Scatter plot showing the relationship between the mean meristem radius and the mean divergence angle.

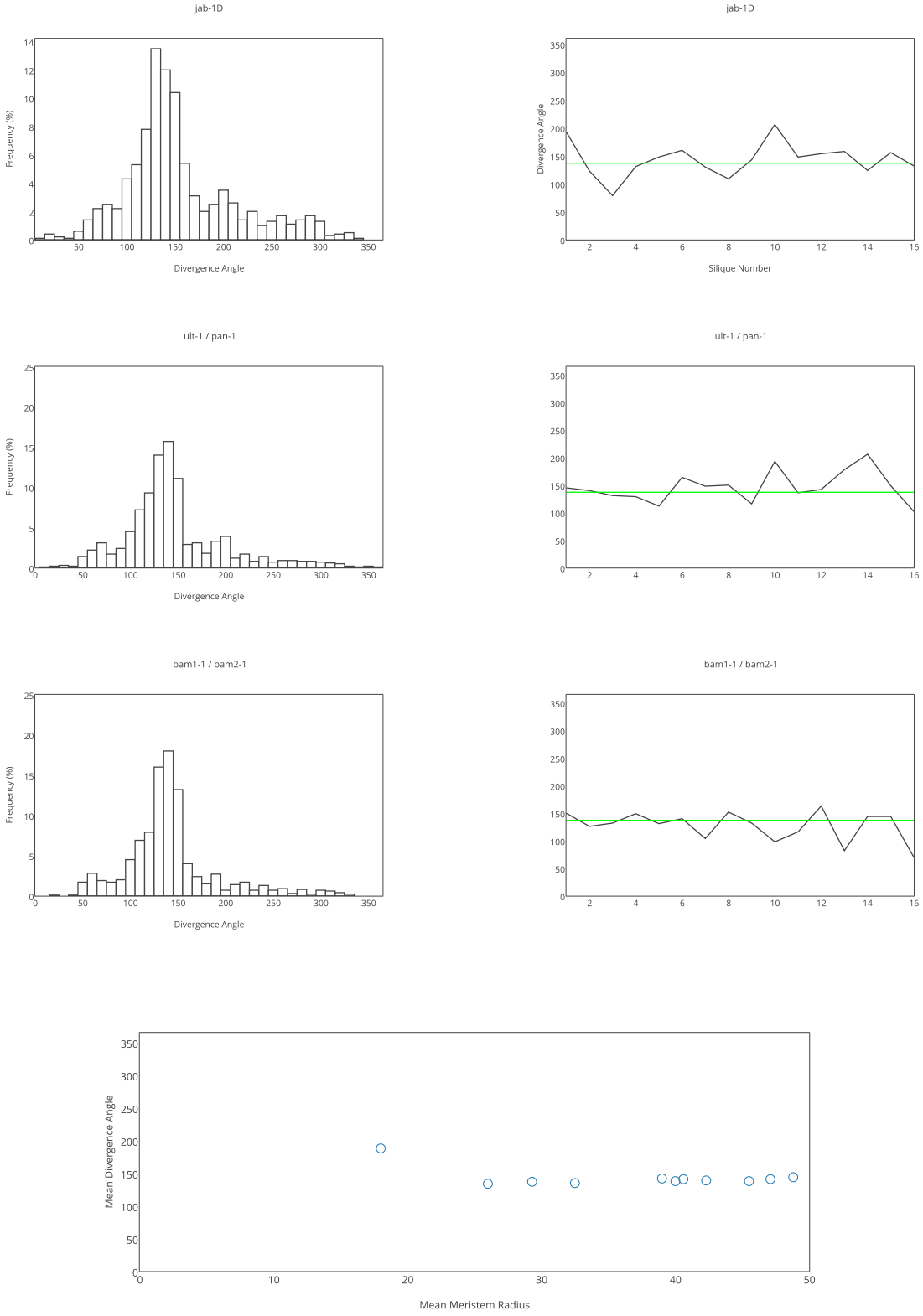

Table 3.2: Mean divergence angle and SAM size Comparison. SAM radius was measured using the saddle-point method rather than the fluorescent marker method. Values are in micrometers. Divergence angles were measured using the divergometer rather than tomography.

Mutant	**Mean Divergence Angle (°)**	**SAM Radius (μm)**
Ler	135	32.5
csld2/3	188	18
plt-3,5,7	137	29.3
ult-1	138	45.5
ult-2	141	47.1
wig-2	138	40
yab3-2 / fil-8	142	39
fil-8	139	42.3
jab-1D	141	40.6
ult-1 / pan-1	144	48.8
bam1-1 / bam2-1	134	26

remarkable phenomenon.

I sought to make sense of this phenomenon first through computer models based on our first principles, then through experiments to probe the predictions made by those models. Using a multi-scale model run on a distributed computing platform I determined that the model parameters most likely to have an effect on the overall phyllotaxis pattern were the size of the cells and the size of the tissue through which the polar auxin transport acts. In the last chapter I experimentally explored the effects of cell size and in this chapter I similarly explored the effect of tissue size on phyllotaxis. To this end, I compared the sizes of SAM with the phyllotaxis patterns in mutants with altered SAM sizes.

In order to accurately quantify the sizes of SAM I explored different measurement methods. The difficultly with measuring the SAM arises from the fact that the SAM does not have a clear boundary. Initially I tired using a fluorescent reporter, the KAN1 promoter driving a nuclear localized GFP, to delineate the edge of the SAM. The KAN1 gene is expressed around the periphery of the SAM and so it theory would make a good marker for the SAM boundary. It would also be relatively simple to quantify using specialized software since the fluorescent nuclei are simple to segment from the cell boundaries. I developed a software work-flow using MorphoGraphX and a small amount of custom software to (1) segment the cells in the SAM and these nuclei, (2) assign cells to either "boundary" or "not boundary" based on the segmented nuclei, and (3) measure the distance in between the boundary region.

This technique, while relatively simple and convenient, had the problem of a high variability. The region of KAN1 expression flip-flops around the floral primordia. At some points around the SAM

it travels in between the SAM and the primordia, at other points it travels around the outside of the primordia, and sometimes it travels around both sides. Since this means that KAN1 does not form a circle around the SAM, picking a single point to measure from is arbitrary and leads to the variability.

To combat this problem, I created a second measurement method based on the topology of the SAM. New primordia form a crease in the surface, or in mathematical terminology, a "saddle point." Since the newest primordia is always approximately the same distance from the center of the SAM across multiple samples and time points, this turned out to be a more reliable method. Compared to the fluorescent reporter method, this method had about 25% as much variability between multiple measurements of different SAMs of the same genetic background. The mean value of the topological method was within 2μm of the fluorescent method.

The second aspect of this study was to measure phyllotaxis angles. In an attempt to make more reliable and repeatable measurements compared to using a divergometer, I developed a photographic technique and software work-flow for generating 3D models of plants and extracting divergence angles from those models. The technique works and makes beautiful 3D pictures but in practice does not increase the repeatability very much. It also takes about two or three times as long to process each plant. While taking measurements using a divergometer requires patients and squinting, the tomography method transfers most of the tedious work to editing 3D meshes on the computer. The time trade-off does not make sense so ultimately I fell back on the divergometer for all my measurements.

The results of comparing meristem size with phyllotaxis pattern show that the mean divergence angle is relatively stable even when the SAM diameter increases 87% (bam1-1/bam2-1 26μm, ult-1/pan-1 48.8μm). Ostensibly this is in contradiction to the model which predicted SAM size to greatly effect phyllotaxis. But the mean divergence angle is not the only metric here. Looking at the distribution of the divergence angles tells a more complex story.

Plants with larger or smaller SAMs than wild type show a wider distribution, or more particularly, a greater quantity distant outliers. So, to a degree, the meristem size is effecting the phyllotaxis, if we assume the correlation is a causal relationship.

One explanation for the lack of diversity in observed phyllotaxis patterns is that phyllotaxis is multistable and we haven't probed a large enough range of SAM sizes to observe the other stable states. In this explanation phyllotaxis is not a gradient and has only a handful of possible states,

which *is* corroborated by the model. In order to see the other states we might need to tweak the geometry of the SAM more. This is evident in the csld2/3 mutant which has a mean SAM diameter of 18μm, the smallest of the mutants considered here, and often produces and alternate phyllotaxis pattern.

Another explanation for the lack of diversity in observed phyllotaxis patterns is that the plant compensates for the altered SAM size in other ways. This is apparent in cell-size mutants (chapter 2). Plants with cells four times as large should have a phyllotaxis pattern similar to csld-2/3 mutants, which have SAMs with approximately one fourth the area as wild type. But those large cell mutants have wild type phyllotaxis. They make up for their larger cells with larger meristems which, if you believe the transport-limited model from chapter 2, makes the meristem the same size from an auxin molecule's point of view. While the meristem-size mutants considered here don't exhibit changes in cell size, one could imagine other aspects of the plant changing to compensate.

This brings up the question of why do plants have such tightly regulated phyllotaxis patterns. One potential answer that I am suggesting is that it's a matter of coincidence. The underlying mechanisms controlling phyllotaxis as proposed in this work are dependent on cell size and tissue size. This connection could have arose purely coincidentally. Since cell size and tissue size are two things that are very tightly regulated in multicellular organisms with multiple layers of redundancies, phyllotaxis can piggy-back on this robustness and become a robust process itself. Robust biological systems are often thought to have arisen through an evolutionary need where individuals expressing a phenotype outside of a narrow range are less fit. For example, individuals with a more loosely coordinated cell cycle may be less fit due to incomplete chromosome replication. But I am proposing that in this particular case a robust phyllotaxis patterning system is not evolutionarily important and arose as a matter of coincidence merely borrowing the robustness of the cell cycle.

Another outstanding question is why 137.5°. There are plenty of proposed answers to this question ranging from the teleological to the numerological. Based on the first principles presented in this work, it appears the answer is that auxin maxima act in a way similar to the inhibitory fields proposed by Alan Turning[11] where organ primordia give off a compound that diffuses through the tissue and inhibits the formation of other primordia in the surrounding region. We now know that the signaling molecule is actually a *positive* regulator rather than a negative one and that it moves *towards* the primordia instead of away. Nevertheless, the outcome is the same and successive primordia are spaced as far from existing primordia as possible, which leads to a scenario where the primordia are optimally spaced with as little undifferentiated tissue as possible, similar to the

conclusions of Douadny and Couder[13]. Successive golden angles (137.5°) also lead an optimal packing scenario around the circumference of a circle. So the connection between organ formation and the golden angle (and subsequently, Fibonacci series) is coincidental in that they both lead to optimal spacing around a circle.

One might suggest that this particular spacing regime is actually an evolutionary feature and polar auxin transport evolved to move auxin "up the gradient" to make leaves optimally packed, providing the plant with a particular fitness. Plenty of people have noticed that optimal spacing of leaves leads to optimal sunlight collection or optimal raindrop collection. None of these explanations make sense. Sunlight capture is very rarely the limiting factor in growth. Nutrients like water, nitrogen, phosphorous, or potassium are in smaller supply. If photosynthesis was the limiting factor, plants could have evolved to capture a larger portion of the spectrum or evolved a more efficient RuBisCO enzyme. If optimally spaced leaves were important for water collection then desert plants should all exhibit the same optimal phyllotaxis pattern but this is not the case.

I am not suggesting that phyllotaxis patterning is completely inconsequential to the plant. In an extreme example, imagine all of the leaves developing on one side of the plant with divergence angle 0°. In this case the meristematic tissue on one side would all develop into leaves while the tissue on the opposite side would all form internode tissue. During shoot bolting this would cause the shoot to severely bend as one side would grow at a much faster rate than the side with the leaves, leading to major morphological problems. This would most likely be evolutionarily disadvantageous. So having a mechanism to prohibit primordia from forming near existing primordia prevents disastrous situations like this from arising and coincidentally leads to Fibonacci spiral patterns.

Of course, this too is speculation and partially teleological. To me it seems to be the simplest explanation given the evidence we have about the underlying mechanism. But our current models are not without limitations. More could be done to understand mechanical force propagation and sensing in the meristem. Our computer models will have to unify our current understanding of polar auxin transport with dynamic tissue growth and new knowledge of cellular and meristem mechanics in order to make progress in this field. Ultimately this will lead to greater understanding of both the molecular scale processes and the overall morphogenesis and development of plants.

References

[1] I Adler. "A History of the Study of Phyllotaxis". In: *Annals of Botany* 80.3 (Sept. 1997), pp. 231–244. ISSN: 03057364.

[2] Johann Wolfgang von Goethe. "Über die Spiraltendenz der Vegetation". In: *Versuch die Metamorphose der Pflanzen zu erklären*. Gotha: Bey Carl Wilhelm Ettinger, 1790.

[3] W Hofmeister. *Allgemeine Morphologie Der Gewachse*. Leipzig: Wilhelm Engelmann, 1868.

[4] Simon Schwendener. *Mechanische Theorie der Blattstellungen*. Leipzig: Wilhelm Engelmann, 1878.

[5] Arthur H Church. *On the relation of phyllotaxis to mechanical laws*. London: Williams & Norgate, 1904.

[6] Mary Snow and R. Snow. "Experiments on Phyllotaxis. I. The Effect of Isolating a Primordium". In: *Philosophical Transactions of the Royal Society of London. Series B* 221 (1932), pp. 1–43.

[7] M. Snow and R. Snow. "Experiments on Phyllotaxis. II. The Effect of Displacing a Primordium". In: *Philosophical Transactions of the Royal Society B: Biological Sciences* 222.483-493 (Jan. 1932), pp. 353–400. ISSN: 0962-8436.

[8] M. Snow and R. Snow. "Experiments on Phyllotaxis. Part III. Diagonal Splits through Decussate Apices". In: *Philosophical Transactions of the Royal Society B: Biological Sciences* 225.519 (May 1935), pp. 63–94. ISSN: 0962-8436.

[9] C. W. Wardlaw. "Organogenesis in Ferns: Evidence Relating to Growth centers and Physiological Fields". In: *Proceedings of the Linnean Society of London* 162.1 (Oct. 1950), pp. 13–18. ISSN: 03700461.

[10] J. C. Schoute. "Beitrage zur Blattstellunglehre. I. Die Theorie". In: *Recueilde Travaux Botániques Néerlandais* 10 (1913), pp. 153–339.

[11] A. M. Turing. "The Chemical Basis of Morphogenesis". In: *Philosophical Transactions of the Royal Society of London. Series B, Biological Sciences,* 237.641 (1952), pp. 37–72.

[12] S. Douady and Y. Couder. "Phyllotaxis as a physical self-organized growth process". In: *Physical Review Letters* 68.13 (Mar. 1992), pp. 2098–2101. ISSN: 0031-9007.

[13] S. Douady and Y. Couder. “Phyllotaxis as a Dynamical Self Organizing Process Part I: The Spiral Modes Resulting from Time-Periodic Iterations”. In: *Journal of Theoretical Biology* 178.3 (Feb. 1996), pp. 255–273. ISSN: 00225193.

[14] S. Douady and Y. Couder. “Phyllotaxis as a Dynamical Self Organizing Process Part II: The Spontaneous Formation of a Periodicity and the Coexistence of Spiral and Whorled Patterns”. In: *Journal of Theoretical Biology* 178.3 (Feb. 1996), pp. 275–294. ISSN: 00225193.

[15] S. Douady and Y. Couder. “Phyllotaxis as a Dynamical Self Organizing Process Part III: The Simulation of the Transient Regimes of Ontogeny”. In: *Journal of Theoretical Biology* 178.3 (Feb. 1996), pp. 295–312. ISSN: 00225193.

[16] F. J. Richards. “Phyllotaxis: Its Quantitative Expression and Relation to Growth in the Apex”. In: *Philosophical Transactions of the Royal Society B: Biological Sciences* 235.629 (Oct. 1951), pp. 509–564. ISSN: 0962-8436.

[17] Paul B Green. “Expression of form and pattern in plants - a role for biophysical fields”. In: *Seminars in Cell & Developmental Biology* 7.6 (1996), pp. 903–911.

[18] Paul B Green. “Pattern Formation in Shoots: A Likely Role for Minimal Energy Configurations of the Tunica”. In: *International Journal of Plant Sciences* 153.3 (1992), S59–S75.

[19] L. F. Hernandez and P. B. Green. “Transductions for the Expression of Structural Pattern: Analysis in Sunflower.” In: *The Plant cell* 5.12 (Dec. 1993), pp. 1725–1738. ISSN: 1532-298X.

[20] J Dumais and CR Steele. “New Evidence for the Role of Mechanical Forces in the Shoot Apical Meristem.” In: *Journal of plant growth regulation* 19.1 (Mar. 2000), pp. 7–18. ISSN: 0721-7595.

[21] P D Shipman and A C Newell. “Polygonal planforms and phyllotaxis on plants.” In: *Journal of theoretical biology* 236.2 (Sept. 2005), pp. 154–97. ISSN: 0022-5193.

[22] Alan C Newell, Patrick D Shipman, and Zhiying Sun. “Phyllotaxis: cooperation and competition between mechanical and biochemical processes.” In: *Journal of Theoretical Biology* 251.3 (2008), pp. 421–39. ISSN: 1095-8541.

[23] K. Okada et al. “Requirement of the Auxin Polar Transport System in Early Stages of Arabidopsis Floral Bud Formation.” In: *The Plant Cell* 3.7 (July 1991), pp. 677–684. ISSN: 1040-4651.

[24] Didier Reinhardt et al. “Regulation of phyllotaxis by polar auxin transport.” In: *Nature* 426.6964 (Nov. 2003), pp. 255–60. ISSN: 1476-4687.

[25] D Reinhardt, T Mandel, and C Kuhlemeier. “Auxin regulates the initiation and radial position of plant lateral organs.” In: *The Plant cell* 12.4 (Apr. 2000), pp. 507–18. ISSN: 1040-4651.

[26] D Reinhardt et al. “Localized upregulation of a new expansin gene predicts the site of leaf formation in the tomato meristem”. In: *Plant Cell* 10.9 (1998), pp. 1427–1437.

[27] Pia A Stieger, Didier Reinhardt, and Cris Kuhlemeier. “The auxin influx carrier is essential for correct leaf positioning.” In: *The Plant Journal* 32.4 (Nov. 2002), pp. 509–17. ISSN: 0960-7412.

[28] Marcus G Heisler et al. “Patterns of auxin transport and gene expression during primordium development revealed by live imaging of the Arabidopsis inflorescence meristem.” In: *Current biology* 15.21 (Nov. 2005), pp. 1899–911. ISSN: 0960-9822.

[29] Olivier Hamant et al. “Developmental patterning by mechanical signals in Arabidopsis.” In: *Science* 322.5908 (Dec. 2008), pp. 1650–5. ISSN: 1095-9203.

[30] Daniel Kierzkowski et al. “Elastic domains regulate growth and organogenesis in the plant shoot apical meristem.” In: *Science* 335.6072 (Mar. 2012), pp. 1096–9. ISSN: 1095-9203.

[31] Benoit Landrein et al. “Meristem size contributes to the robustness of phyllotaxis in Arabidopsis.” In: *Journal of experimental botany* 66.5 (Mar. 2015), pp. 1317–24. ISSN: 1460-2431.

[32] S P Venglat et al. “The homeobox gene BREVIPEDICELLUS is a key regulator of inflorescence architecture in Arabidopsis.” In: *Proceedings of the National Academy of Sciences of the United States of America* 99.7 (Apr. 2002), pp. 4730–5. ISSN: 0027-8424.

[33] A Bogner et al. “A history of scanning electron microscopy developments: towards "wet-STEM" imaging.” In: *Micron (Oxford, England : 1993)* 38.4 (Jan. 2007), pp. 390–401. ISSN: 0968-4328.

[34] P. J. Breton. “From Microns to Nanometers: Early Landmarks in the Science of Scanning Electron Microscope Imaging”. In: *Scanning Microscopy* 13.1 (1999), pp. 1–6.

[35] John N. Owens and Marje Molder. “A study of DNA and mitotic activity in the vegetative apex of Douglas fir during the annual growth cycle”. en. In: *Canadian Journal of Botany* 51.7 (Jan. 1973), pp. 1395–1409.

[36] Paul B. Green and Kenton E. Brooks. “Stem Formation from a Succulent Leaf: Its Bearing on Theories of Axiation”. In: *American Journal of Botany* 65.1 (1978), pp. 13–26.

[37] S. J. Owens and N. J. Horsfield. “A light and electron microscopic study of stigmas in Aneilema and Commelina species (Commelinaceae)”. In: *Protoplasma* 112.1-2 (Feb. 1982), pp. 26–36. ISSN: 0033-183X.

[38] John S. Gardner, W. M. Hess, and E. J Trione. “Development of the Young Wheat Spike: A Sem Study of Chinese Spring Wheat”. In: *American Journal of Botany* 72.4 (1985), pp. 548–559.

[39] Lisa Morrison Baird, Margaret Jorgensen Turano, and Barbara D. Webster. “Ultrastructural and Histochemical Characteristics of the Stigma of Cicer arietinum”. In: *American Journal of Botany* 75.4 (1988), pp. 551–557.

[40] M.H Williams, M Vesk, and M.G Mullins. “Tissue preparation for scanning electron microscopy of fruit surfaces: Comparison of fresh and cryopreserved specimens and replicas of banana peel”. In: *Micron and Microscopica Acta* 18.1 (Jan. 1987), pp. 27–31. ISSN: 07396260.

[41] J Marc and W P Hackett. “Changes in the pattern of cell arrangement at the surface of the shoot apical meristem in Hedera helix L. following gibberellin treatment.” In: *Planta* 186.4 (Mar. 1992), pp. 503–10. ISSN: 0032-0935.

[42] M. H. Williams and P. B. Green. “Sequential scanning electron microscopy of a growing plant meristem”. In: *Protoplasma* 147.1 (Feb. 1988), pp. 77–79. ISSN: 0033-183X.

[43] T A Klar and S W Hell. “Subdiffraction resolution in far-field fluorescence microscopy.” In: *Optics letters* 24.14 (July 1999), pp. 954–6. ISSN: 0146-9592.

[44] Eric Betzig et al. “Imaging intracellular fluorescent proteins at nanometer resolution.” In: *Science* 313.5793 (Sept. 2006), pp. 1642–5. ISSN: 1095-9203.

[45] Pierre Barbier de Reuille et al. “MorphoGraphX: A platform for quantifying morphogenesis in 4D.” In: *eLife* 4 (Jan. 2015), p. 05864. ISSN: 2050-084X.

[46] Magalie Uyttewaal et al. “Mechanical stress acts via katanin to amplify differences in growth rate between adjacent cells in Arabidopsis.” In: *Cell* 149.2 (Apr. 2012), pp. 439–51. ISSN: 1097-4172.

[47] S Webb. *From the Watching of Shadows: The Origins of Radiological Tomography*. 1st Editio. Boca Raton, FL: CRC Press, 1990, p. 347. ISBN: 085274305X.

[48] B. Pollak. “Experiences with Planography”. In: *CHEST Journal* 24.6 (Dec. 1953), p. 663. ISSN: 0012-3692.

[49] T. J. Littleton and M. L. Durzizch Littleton. “Conventional Tomography”. In: *A History of the Radiological Sciences*. Reston, VA: Radiology Centennial, Inc, 1996. Chap. 15, p. 369401.

[50] H Hornich. “A tnrbute to Johann radon.” English. In: *IEEE transactions on medical imaging* 5.4 (Jan. 1986), p. 169. ISSN: 0278-0062.

[51] M S Smyth and J H Martin. “x ray crystallography.” In: *Molecular pathology : MP* 53.1 (Feb. 2000), pp. 8–14. ISSN: 1366-8714.

[52] Romain Fernandez et al. “Imaging plant growth in 4D: robust tissue reconstruction and lineaging at cell resolution.” In: *Nature Methods* May (June 2010). ISSN: 1548-7105.

[53] Scott L. Delp, Anthony M. DiGoia, and Branislav Jaramaz, eds. *Medical Image Computing and Computer-Assisted Intervention – MICCAI 2000*. Vol. 1935. Lecture Notes in Computer Science. Berlin, Heidelberg: Springer Berlin Heidelberg, 2000. ISBN: 978-3-540-41189-5.

[54] O Commowick and G Malandain. “Evaluation of Atlas Construction Strategies in the Context of Radiotherapy Planning”. In: *Proceedings of the SA2PM Workshop (From Statistical Atlases to Personalized Models)*. Copenhagen, 2006, pp. 1–4.

[55] Liselott Slot, Peter K Larsen, and Niels Lynnerup. “Photogrammetric documentation of regions of interest at autopsy–a pilot study.” In: *Journal of forensic sciences* 59.1 (Jan. 2014), pp. 226–30. ISSN: 1556-4029.

[56] F. Chiabrando et al. “Very close nadiral images: a proposal for quick digging survey”. In: *International Archives of Photogrammetry* XXXVIII.5 (2010), pp. 155–160. ISSN: 15740846.

[57] Paz Merelo et al. “Genome-wide identification of KANADI1 target genes.” In: *PloS one* 8.10 (Jan. 2013), e77341. ISSN: 1932-6203.

[58] E. W. Dijkstra. “A note on two problems in connexion with graphs”. In: *Numerische Mathematik* 1.1 (Dec. 1959), pp. 269–271. ISSN: 0029-599X.